

DTIC FILE COPY

Send J



# SANDIA REPORT

SAND86-2492 • UC-70

Unlimited Release

Printed July 1987

## AD-A204 274

# Microstructure of Red Clay From the Central Pacific Deep-Sea Basin: Significance to Subseabed Nuclear Waste Disposal

P. J. Burkett, R. H. Bennett, H. Li, F. L. Nastav, W. R. Bryant, L. E. Shephard, Wen-An Chiou

Prepared by  
Sandia National Laboratories  
Albuquerque, New Mexico 87185 and Livermore, California 94550  
for the United States Department of Energy  
under Contract DE-AC04-76DP00789

DTIC  
ELECTE  
S 7 FEB 1989 D  
E

A



SF2900Q(8-81)

This report has been approved for public release and sale in its entirety as authorized by DTIC. Distribution is unlimited. DTIC

Issued by Sandia National Laboratories, operated for the United States Department of Energy by Sandia Corporation.

**NOTICE:** This report was prepared as an account of work sponsored by an agency of the United States Government. Neither the United States Government nor any agency thereof, nor any of their employees, nor any of their contractors, subcontractors, or their employees, makes any warranty, express or implied, or assumes any legal liability or responsibility for the accuracy, completeness, or usefulness of any information, apparatus, product, or process disclosed, or represents that its use would not infringe privately owned rights. Reference herein to any specific commercial product, process, or service by trade name, trademark, manufacturer, or otherwise, does not necessarily constitute or imply its endorsement, recommendation, or favoring by the United States Government, any agency thereof or any of their contractors or subcontractors. The views and opinions expressed herein do not necessarily state or reflect those of the United States Government, any agency thereof or any of their contractors or subcontractors.

Printed in the United States of America  
Available from  
National Technical Information Service  
U.S. Department of Commerce  
5285 Port Royal Road  
Springfield, VA 22161

NTIS price codes  
Printed copy: A03  
Microfiche copy: A01

**REPORT DOCUMENTATION PAGE**

1a. REPORT SECURITY CLASSIFICATION <u>Unclassified</u>			1b. RESTRICTIVE MARKINGS <u>None</u>			
2a. SECURITY CLASSIFICATION AUTHORITY			3. DISTRIBUTION / AVAILABILITY OF REPORT Approved for public release; Distribution is unlimited			
2b. DECLASSIFICATION / DOWNGRADING SCHEDULE						
4. PERFORMING ORGANIZATION REPORT NUMBER(S)			5. MONITORING ORGANIZATION REPORT NUMBER(S)			
6a. NAME OF PERFORMING ORGANIZATION Naval Ocean Research and Development Activity		6b. OFFICE SYMBOL (if applicable) 360	7a. NAME OF MONITORING ORGANIZATION Naval Ocean Research and Development Activity			
6c. ADDRESS (City, State, and ZIP Code) Ocean Scienc Directorate Stennis Space Center, MS 39529-5004			7b. ADDRESS (City, State, and ZIP Code) Ocean Science Directorate Stennis Space Center, MS 39529-5004			
8a. NAME OF FUNDING / SPONSORING ORGANIZATION Sandia Nat'l Labs. (DOE)		8b. OFFICE SYMBOL (if applicable) (DOE)	9. PROCUREMENT INSTRUMENT IDENTIFICATION NUMBER			
8c. ADDRESS (City, State, and ZIP Code) Albuquerque, N.M.			10. SOURCE OF FUNDING NUMBERS			
			PROGRAM ELEMENT NO. 920101	PROJECT NO. 00101	TASK NO. 421	WORK UNIT ACCESSION NO. DN394444
11. TITLE (Include Security Classification) Microstructure of Red Clay From the Central Pacific Deep-Sea Basin: Significance to Subseabed Nuclear Waste Disposal						
12. PERSONAL AUTHOR(S) P. I. Burkett, R. H. Bennett, H. J. E. L. Nastay, W. R. Bryant, L. E. Shephard, Wen-An Chiu						
13a. TYPE OF REPORT <u>Journal Article</u>		13b. TIME COVERED FROM _____ TO _____		14. DATE OF REPORT (Year, Month, Day) <u>July 1987</u>		
15. PAGE COUNT <u>1</u>						
16. SUPPLEMENTARY NOTATION						
17. COSATI CODES			18. SUBJECT TERMS (Continue on reverse if necessary and identify by block number) significance of clay microstructure to nuclear waste disposal clay microstructure			
FIELD	GROUP	SUB-GROUP				
19. ABSTRACT (Continue on reverse if necessary and identify by block number) See attached paper						
20. DISTRIBUTION / AVAILABILITY OF ABSTRACT <input type="checkbox"/> UNCLASSIFIED/UNLIMITED <input checked="" type="checkbox"/> SAME AS RPT. <input type="checkbox"/> DTIC USERS			21. ABSTRACT SECURITY CLASSIFICATION <u>Unclassified</u>			
22a. NAME OF RESPONSIBLE INDIVIDUAL <u>R. H. Bennett</u>			22b. TELEPHONE (Include Area Code) <u>(601) 688-5460</u>		22c. OFFICE SYMBOL <u>360</u>	

**MICROSTRUCTURE OF RED CLAY  
FROM THE CENTRAL PACIFIC DEEP-SEA BASIN:  
SIGNIFICANCE TO SUBSEABED NUCLEAR WASTE DISPOSAL**

P. J. Burkett, R. H. Bennett, H. Li, and F. L. Nastav  
Naval Ocean Research and Development Activity

W. R. Bryant  
Texas A&M University  
College Station, TX 77843

L. E. Shephard  
Sandia National Laboratories  
Albuquerque, NM 87185

Wen-An Chiou  
Northwestern University  
Evanston, IL 60201

↓  
**ABSTRACT**

The microstructure of deep-sea illitic red clay from the central Pacific Basin was investigated using transmission and scanning electron microscopy techniques. Gravity core samples ("undisturbed") and sediments from dredge hauls ("disturbed") were used in the investigations and analysis. Dredged samples were remolded and reconsolidated to equivalent in situ porosities by geotechnical engineers from the University of Rhode Island for use in a scaled simulation test for the Subseabed Disposal Program, Sandia National Laboratories. This study was part of the In Situ Heat Transfer Experiment simulation test designed to investigate the thermal, fluid, mechanical, and chemical response of the sediment to a heater emplaced in the seabed. The clay fabric of the undisturbed core samples was compared with that of the remolded, reconsolidated sediment to investigate the effects of remolding, the mechanical disturbance due to the

insertion of probes, and the induced thermal gradients due to heating of the sediment. (mgm) ←

To a first approximation, no significant difference in the fabric was observed between the undisturbed and remolded illitic sediment. Samples adjacent to the heater probe were subjected to temperatures slightly below 300°C. Slight preferential clay particle alignment probably resulting from shearing stresses developed in the sediment during probe insertion. Heating of the sediment did not appear to have a significant effect on the fabric, with the exception of localized "quasi-expansion" and flow features observed in the microfabric in the near field.

The undisturbed sediment fabric of the RAMA samples displayed a random arrangement of particles. The fabric is composed of a complex assemblage of particles having a matrix consisting predominately of  $\leq 1 \mu\text{m}$  domains and small particles. Characteristic features of this high void ratio

sediment forming the microfabric are larger 2- to 5- $\mu$ m illitic domains (fractured during ultra-thin sectioning), stepped face-to-face and end-to-end short chains, various aggregate types (including large intra-void and denser aggregates), and channels for fluid transport. A significant portion of illite, the dominant mineral, appears to be a product of aeolian processes originating from argillites of eastern Asia. Chlorite, kaolinite, smectite, and quartz are minor constituents. Aggregates of finely divided particulate material having intra-voids maintain structural integrity in spite of remolding in the laboratory. The surficial illitic-rich red clay can be reconstituted easily in the laboratory; thus, this remolded sediment appears to

be a suitable material for geotechnical laboratory tests simulating in situ conditions.

#### ACKNOWLEDGEMENT

The authors wish to thank Gail Romero, Naval Ocean Research and Development Activity (NORDA), for laboratory assistance and for providing initial scanning electron microscope photomicrographs. We also thank Dr. C. Mark Percival for providing the electron microscope subsamples. The project was funded by Sandia National Laboratories' Subseabed Disposal Program and supplemental funds were provided by NORDA to support P. J. Burkett and R. H. Bennett during this study.

**CONTENTS**

<b>INTRODUCTION</b> .....	1
<b>BACKGROUND</b> .....	1
<b>METHODS AND MATERIALS</b> .....	4
Coring and Subsampling.....	4
Geotechnical and Thermal Probes.....	5
Grain-Size Determination.....	6
Clay Fabric Preparation Techniques.....	6
Critical Point Drying.....	7
Embedding.....	8
Rose Diagram.....	8
X-Ray Diffraction.....	15
<b>RESULTS AND DISCUSSION</b> .....	15
Thermal Effects.....	15
Mechanical Disturbance.....	18
Grain Size Analysis.....	22
X-Ray Mineralogy: Pre- and Post-ISIMU.....	22
Fabric Analysis.....	24
<b>CONCLUSIONS</b> .....	36
<b>REFERENCES</b> .....	39

<b>Accession For</b>	
NTIS GRA&I	<input checked="" type="checkbox"/>
DTIC TAB	<input type="checkbox"/>
Unannounced	<input type="checkbox"/>
Justification	
By	
Distribution/	
<b>Availability Codes</b>	
<b>Dist</b>	<b>Avail and/or Special</b>
A-1	



## FIGURES

1.	Particle Arrangements Comprising Clay Fabric.....	2
2.	Locale in the Northwest Pacific of the MPG-1 Site from Which RAMA Samples Were Taken.....	3
3.	ISIMU Test Tank Setup with Reconstituted Illitic Sediment Subject to Equivalent Deep-Sea Ambient Pressure in a Hyperbaric Chamber.....	4
4.	Cross Section of ISHTE Simulation (ISIMU) Tank.....	5
5.	Diagram Showing Position of ISIMU Heater Probe in Relation to Piston Cores 1 and 2, and the Subsamples Used for Clay Fabric Analysis.....	5
6.	Sample B-4: Rose Diagram (A), Frequency Histogram (B), and TEM Micrograph (C) Showing Bimodal Distribution of Particles.....	9
7.	Sample B-5: Rose Diagram (A), Frequency Histogram (B), and TEM Micrograph (C) Showing Some Preferred Particle Orientations Similar to a Normal Gaussian Distribution.....	10
8.	Sample B-7: Rose Diagram (A), Frequency Histogram (B), and TEM Micrograph (C) Showing a Slightly Bimodal Distribution of Particles.....	11
9.	RAMA Sample: Rose Diagram (A), Frequency Histogram (B), and TEM Micrograph (C) Showing a Slight Particle Orientation Preference.....	12
10.	RAMA Mosaic.....	13
11.	Rose Diagram (A) and Frequency Histogram (B) for RAMA Mosaic Showing a Completely Random Distribution of Particle Arrangements.....	16
12.	Steady-State Isotherm Showing Position of 12 Fabric Samples, and the Cusp Samples Used for X-Ray Diffraction Analysis.....	17
13.	Water Content Versus Depth Profile for ISIMU Post-Test Samples Showing Water Content Minimum Corresponding to the End of the Heater Probe.....	19
14.	Water Content Versus Distance from the Inconel Heat Source at a Depth of 24.6-28.8 cm.....	20
15.	ISHTE Simulation Combined Profile.....	20
16.	A) Models of Complex Soil Disturbance Patterns Resulting from Pile Insertion; B) Zones of Plastic and Elastic Deformation Resulting from Pile Insertion; C) Deformation Patterns Resulting from "Simple Pile" Penetration.....	21
17.	Grain Size Comparison of RAMA Sample to Sample PC-5, Which Was Remolded and Laboratory-Consolidated to Equivalent In Situ Porosity.....	23
18.	X-Ray Diffraction Pattern Showing Pronounced Increase in the Smectite Peak Occurring at the 27- and 33-cm Depths.....	24
19.	Probe Insertion Disturbance Features.....	25
20.	Probe Insertion Disturbance Features.....	26
21.	A) Primary Remolding Causing Swirling of Domains and Forming Voids Performing as Pathways for Pore Fluids and Small Particle Transport; B) Enlargement of Chain of Domains Bent During Remolding; C) The Less-Dense Fabric of a RAMA Sample, Not Subjected to Remolding or Probe Insertion Stress, Demonstrating Characteristic Straight, Long Chains of Domains.....	27

**FIGURES (Continued)**

22.	Cross Sections of Quasi-Expansion Features in Near-Field Samples B-7, B-8, and B-10, Which Have Voids Acting as Conduits for Pore Fluids.....	29
23.	Low-Density Smectite Aggregate of Sample B-1 Demonstrating the Onion Skin Layering of Particles Typical of Heated Fabric Samples.....	30
24.	A) Sample B-3 Shows a Low-Density Aggregate, Probably Smectite, Surrounded by Onion Skin Layering of EE and EF Particles, Beyond Which are Channels for Pore Fluid Transport; B) Small Particles and Domains Line the Low-Density Aggregate.....	31
25.	Proposed Tentative Clay Fabric Models for Submarine Sediment.....	32
26.	High Void Ratio nonRemolded Fabric of In Situ RAMA Sample Showing Micro-Channels.....	33
27.	A Large Subrounded Argillite Indicative of Aeolian Origin.....	34
28.	SEM Micrograph of Features Recognizable in Both SEM and TEM.....	35

## ACRONYMS/ABBREVIATIONS

CEC	cation exchange capacity
CPD	critical point drying
DSDP	Deep Sea Drilling Project
EE	edge to edge
EF	edge to face
FF	face to face
F.Z.	fracture zone
ISHTe	In Situ Heat Transfer Experiment
ISIMU	In Situ Heat Transfer Experiment Simulation
ISV	in situ vane
MPG-1	central Pacific Ocean sampling site
NORDA	Naval Ocean Research and Development Activity
RAMA	undisturbed clay sediment from the MPG-1 site
SDP	Subseabed Disposal Program
SEM	scanning electron microscopy/microscope
SMTS	seamounts
TEM	transmission electron microscopy/microscope
TR	trough

# MICROSTRUCTURE OF RED CLAY FROM THE CENTRAL PACIFIC DEEP-SEA BASIN: SIGNIFICANCE TO SUBSEABED NUCLEAR WASTE DISPOSAL

## INTRODUCTION

The study of clay microstructure, defined as the fabric of the sediments and the physico-chemical interactions among its components, is fundamental to the investigation of fine-grained sediments. Clay "fabric" refers to the spatial distributions, orientations, and particle-to-particle relationships of the solid particles (generally those less than 3.9 microns in size); physico-chemical interactions are the expressions of the forces active among the particles. An understanding of the relationships between clay fabric and the physico-chemical interactions of the sediments is essential to the study of fine-grained sediments, diagenesis, and ultimately shales and argillites. Because clay microstructure is an important fundamental sediment property, basic investigations of this aspect are vital to understanding the behavior and response of sediments to static and dynamic loads in practical applications.

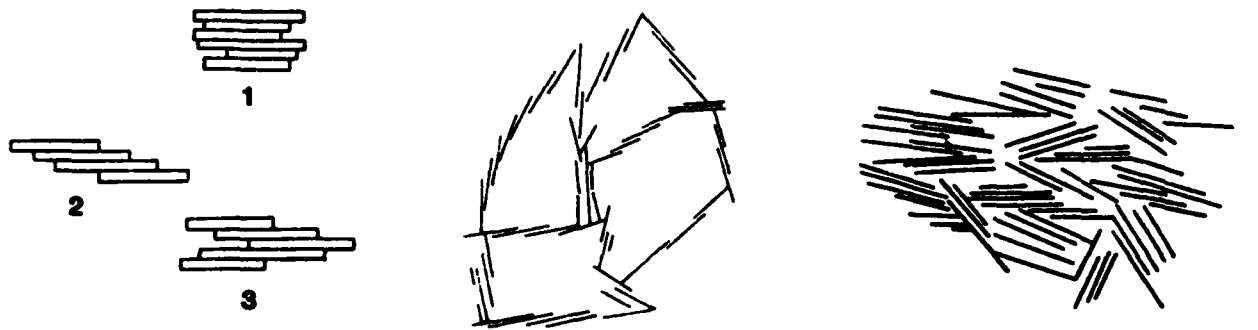
Several terms are used to qualitatively describe the clay fabric. A particle is the elementary unit that can be resolved by the transmission electron microscope (TEM). Particles consist of single clay platelets or several platelets which form domains. Domains are stacks of parallel clay plates arranged face-to-face, slightly stepped, or in similar configurations (Bennett, 1976; Bennett and Hulbert, 1986). An array of domains is referred to as turbostratic fabric (Aylmore and Quirk, 1960). Aggregates generally consist of a very porous network of randomly-oriented clay flakes. These also can be referred to as well-defined clay aggregates composed of several particles or domains. A chain is a series of clay particles or domains that are linked together and may have several arrangements of contact points

in a chain. For example, short-stepped, face-to-face chains or edge-to-edge particle contacts or a combination of these features are common (Figure 1). Chains sometimes can be relatively long.

The objective of this investigation was to study the fabric of red clay sediments from the central Pacific deep-sea basin using transmission electron microscopy (TEM), and to assess sediment response to thermal and mechanical effects that may result from radioactive waste disposal. The samples analyzed were cored from remolded, laboratory-consolidated, illitic-rich red clay used in the In Situ Heat Transfer Experiment Simulation (ISIMU) test (Percival, 1982). The fabric of these samples was compared to undisturbed samples, designated RAMA, which were obtained with a gravity core from the MPG-1 site in the central Pacific Ocean (Figure 2). Specific objectives of this study included an analysis of the fabric characteristics as a result of: 1) mechanical disturbances from remolding and heater probe insertion; 2) induced thermal gradients from heating of the sediment; 3) changes in physical properties, such as undrained shear strength, water content, void ratio, and mineralogy.

## BACKGROUND

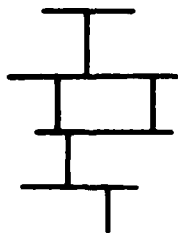
The Subseabed Disposal Program (SDP) is evaluating the feasibility of emplacing high-level radioactive waste in fine-grained sediments of the world ocean basins (Hollister et al., 1981; Percival, 1983). The In Situ Heat Transfer Experiment (ISHTE) is a phase of the SDP designed to provide data on the in situ thermal, fluid dynamic, thermochemical, and mechanical response of sediment to the emplacement of



A. Domain structures (Moon, 1972): 1) "book" (Sloan and Kell, 1966); 2) "stepped;" 3) face-to-face (FF) (Smalley and Cabrera, 1969).

B. Chain of stepped, FF, and edge-to-edge (EE) particles (O'Brien, 1971).

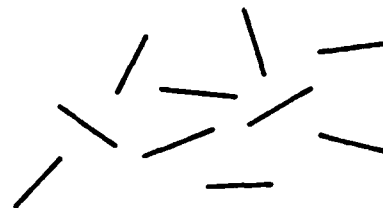
C. "Turbostratic" structure (Aylmore and Quirk, 1960).



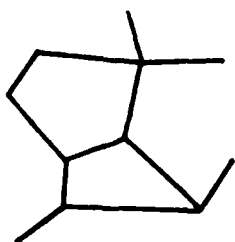
D. Dispersed and deflocculated (van Olphen, 1963).



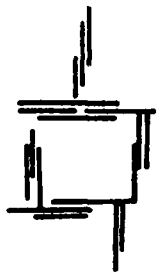
E. Aggregated, but deflocculated (van Olphen, 1963).



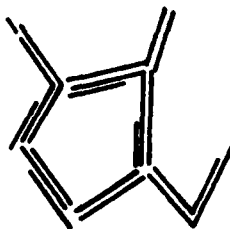
F. Edge-to-face (EF), flocculated, but dispersed (van Olphen, 1963).



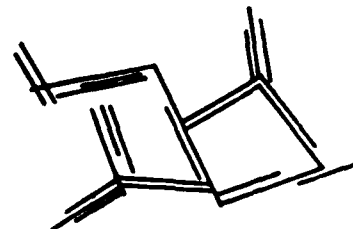
G. EE flocculated, but dispersed (van Olphen, 1963).



H. EF, flocculated, and aggregated (van Olphen, 1963).



I. EE flocculated, but aggregated (van Olphen, 1963).



J. EF and EE flocculated and aggregated (van Olphen, 1963).

Figure 1. Particle Arrangements Comprising Clay Fabric (Redrawn from Bennett et al., 1977).

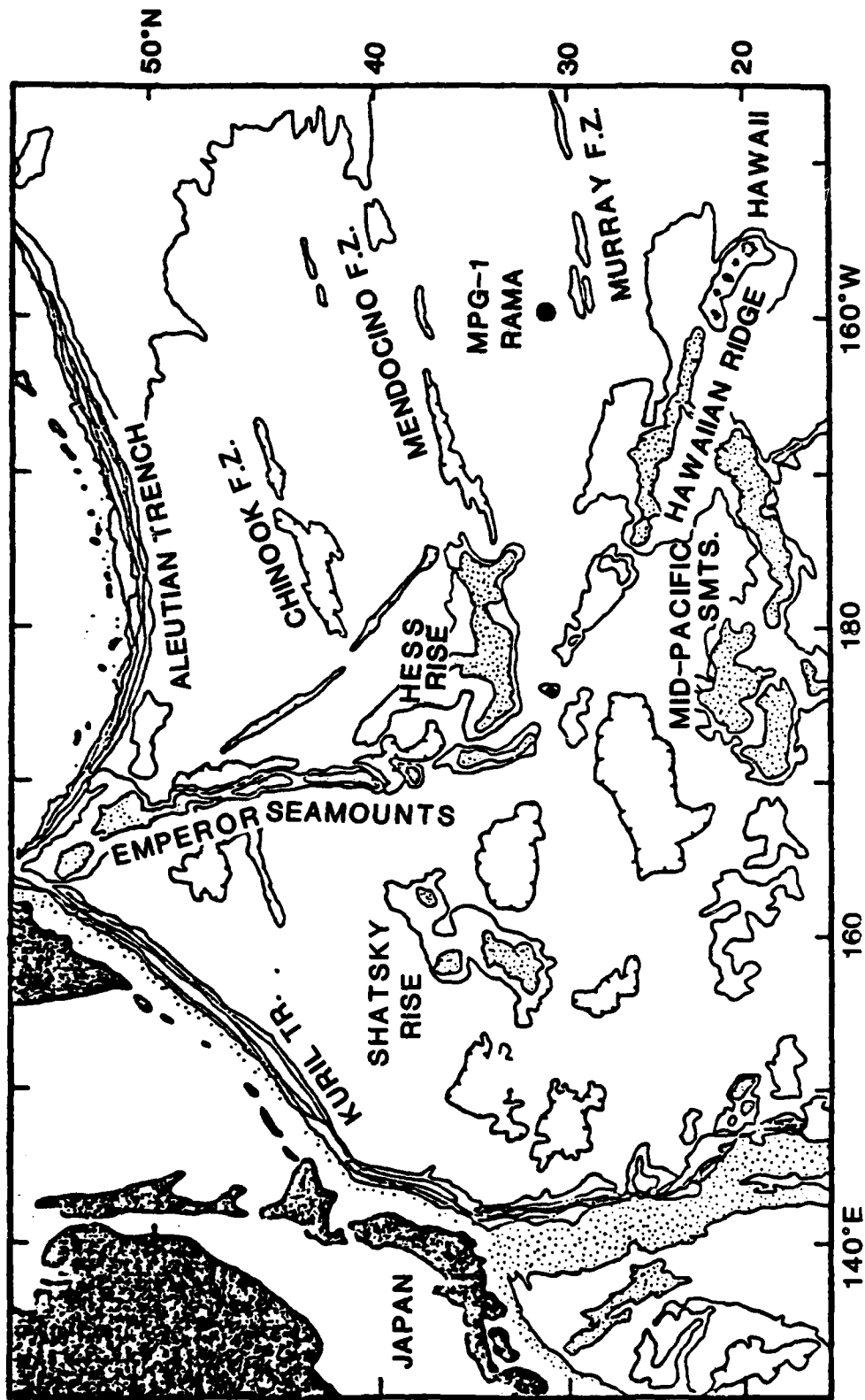


Figure 2. Locale in the Northwest Pacific Ocean of the MPG-1 Site from Which RAMA Samples Were Taken (Redrawn from DSDP Leg 86 Site Map).

radioactive waste in the seabed. Measurements of the thermal response of the sediment will be compared with numerical predictions to validate a thermomechanical model for deep-sea sediments (Olson and Harrison, 1979; Percival et al., 1980). An integral part of ISHTE is the development and demonstration of the technology required to perform waste isolation experiments in the seabed in water depths of 6000 m (Percival et al., 1980). A scaled laboratory simulation experiment (ISIMU) was conducted in 1981 by Sandia National Laboratories and participating institutions (Percival, 1982). ISIMU was designed to simulate predicted environmental field conditions and to test some of the instruments that will eventually be part of the full-scale ISHTE. The test was performed in a 1-m<sup>3</sup> cylindrical container filled with remolded, reconsolidated, illitic pelagic clay recovered by dredge hauls from the proposed ISHTE test site in the central Pacific (Figure 3; Silva et al., 1983). ISIMU was conducted in a hyperbaric chamber at the David Taylor Naval Ship Research and Development Center, Annapolis, Maryland. A calculated scale of approximately 0.28:1.0 allowed adequate thermal equilibrium to be reached within one month. The dredged sediment was reconstituted in a rotary mixer with 34.2 ‰ salinity seawater until a homogeneous slurry was formed. A series of thin (approximately 20-cm) layers of the slurry were added to the tank, and a vacuum was applied to each layer to remove excess air. Reconsolidation, over a ten-week period, simulated in situ porosities of the deep ocean sediments (Silva et al., 1983). The tank, sediments, and emplaced instrumentation were pressurized to 55 MPa at 4°C and experiments were run for one month. Additional details of the simulation test can be found in Applied Physics Laboratory, University of Washington (1982), Silva et al. (1983), Percival (1982), and Bennett et al. (1985).

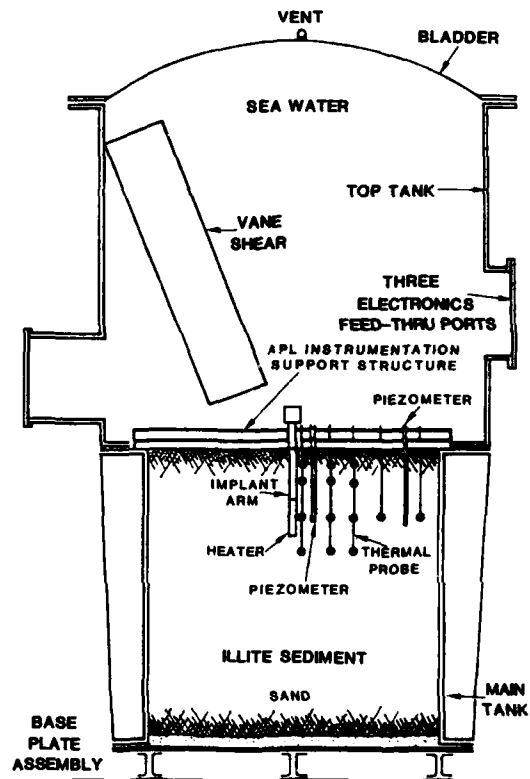


Figure 3. ISIMU Test Tank Setup with Reconstituted Illitic Sediment Subject to Equivalent Deep-Sea Ambient Pressure in a Hyperbaric Chamber (Redrawn from Silva, 1983).

## METHODS AND MATERIALS

### Coring and Subsampling

After high-pressure ISIMU testing, two 10-cm-diameter cores were obtained for fabric analysis (Figure 4). Core PC-1 was located at the center of the tank adjacent to core PC-2. A 7.5-cm-diameter core, PC-3, was collected 40 cm from the center (Figure 4). The area between the three cores is referred to as the cusp. The edge of a 10-cm-diameter core, PC-5, located 33 cm from the center of the tank and

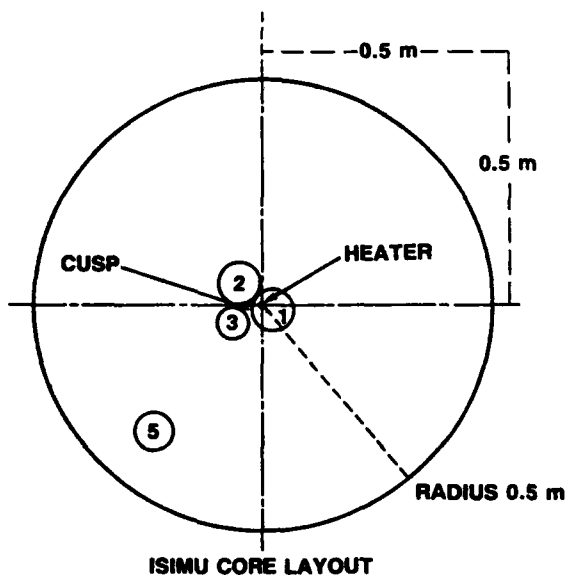


Figure 4. Cross Section of ISHTE Simulation (ISIMU) Tank. Fabric samples were obtained from Cores PC-1 and PC-2. X-ray diffraction was performed on samples from the cusp located between Cores 1, 2, and 3.

outside the heated region, was used for grain size analysis. Twelve subsamples (16 cm<sup>3</sup>) were collected normal to the longitudinal axis of cores PC-1 and PC-2 at selected distances from the heater's edge and at measured depths below the mudline (Figure 5; Table 1). The RAMA control samples were subcored from undisturbed gravity core samples obtained from the MPG-1 site (Figure 2).

#### Geotechnical and Thermal Probes

The physical and mechanical properties of the ISIMU cores were analyzed by the University of Rhode Island/Marine Geomechanics Laboratory (Silva et al., 1983). Laboratory analyses were performed on sediment samples obtained prior to and after heating. These analyses included water

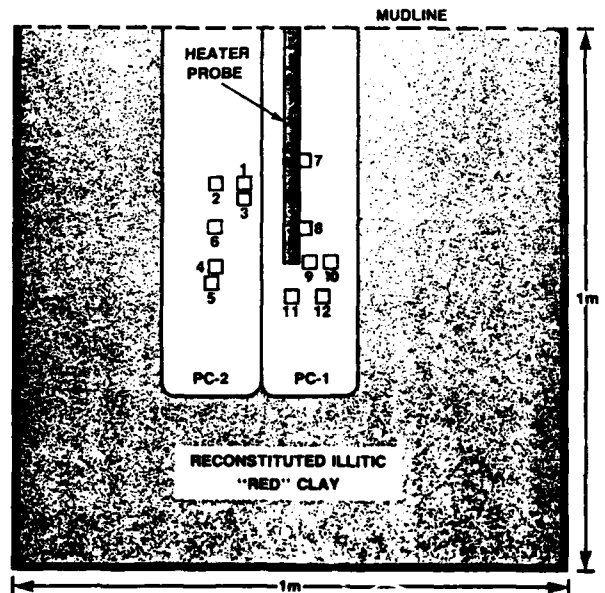


Figure 5. Diagram Showing Position of ISIMU Heater Probe in Relation to Piston Cores 1 and 2, and the Sub-Samples Used for Clay Fabric Analysis.

Table 1  
ISIMU FABRIC SAMPLES

Sample #	Core #	Depth below Mudline (cm)	Distance from Heater Edge (cm)
B-1	PC2	21.4-22.9	1.5
B-2	PC2	21.4-22.9	5.5
B-3	PC2	23.1-24.6	1.5
B-4	PC2	33.4-34.9	5.5
B-5	PC2	35.9-37.4	6.0
B-6	PC2	27.5-28.0	5.5
B-7	PC1	18.1-19.6	0.0
B-8	PC1	27.8-29.3	0.0
B-9	PC1	32.8-34.3	0.5
B-10	PC1	32.8-34.3	3.5
B-11	PC1	37.3-38.8	directly under heater
B-12	PC1	37.3-38.8	2.5

content, consolidation, and triaxial compression tests. An in situ vane (ISV) device developed by the University of Rhode Island measured sediment shear strength under in situ pressure and temperature conditions during ISIMU. The ISV system consists of a vane shear probe contained in a pressure-compensated, oil-filled housing with a microprocessor control system, and a rechargeable power supply (Silva et al., 1983). NORDA's two in situ piezometer probes use an 8-mm-diameter titanium tube and a 5-degree cone probe tip. The piezometer pressure transducers operate at ambient hydrostatic pressure (69 MPa) (Bennett et al., 1985). During testing, the heater probe experienced a temperature differential along its length ranging from 4 to 300°C. Different types of thermal probes for measuring sediment and water temperatures were used by the University of Washington/Applied Physics Laboratory (Miller et al., 1982). These probes included: five Sea-Bird Electronic Model SBE-3 oceanographic thermometers; four ARI Industries multilevel probes, each consisting of four thermocouples in a single assembly for near-field measurements; four standard Conax Corporation thermocouples for far-field measurements.

#### Grain-Size Determination

A remolded, laboratory-reconsolidated sample from core PC-5 and RAMA control samples were analyzed for grain-size using Micromeritics Model 5000 particle size analyzer for the 4- to 10-phi, silt and clay-size fractions (grain-size expressed in phi [ $\phi$ ] is equal to the negative log to the base two of the grain diameter in millimeters; i.e.,  $\phi = -\log_2 D[\text{mm}]$ ; Krumbein, 1934). The sediments were soaked in 2.5-g/L sodium hexametaphosphate dispersant, then disaggregated using a sonic energy cell disruptor for 12 minutes while stirring with a magnetic stirrer (Briggs, 1984). Wet sieving through a 62- $\mu\text{m}$  screen separated the fine (silt and clay) and

coarse (sand) fractions. The coarse fraction was dried and weighed, and the fines were brought to 1000-mL volume with the dispersant, and vigorously stirred and aerated. A 20-mL aliquot, representing the total distribution of particles in suspension, was pipetted, dried, and weighed for a total percent solids determination. After five days of settling, other 20-mL aliquots were pipetted at designated depths, dried, and weighed to estimate the weight of clay-size particles in the 10- to 14-phi intervals. After six days of settling, the bottom of the cylinder contained all particles coarser than 10 phi. The supernatant was carefully siphoned and the volume recorded. A 20-mL subsample was dried and weighed for an estimate of the total particles finer than 10 phi. The particles and about 200 mL of dispersant remaining in the graduated cylinder were disaggregated, stirred for 12 minutes, and the size was determined using the Micromeritics analyzer. The concentration of silt-size and clay-size particles in liquid suspension at various depths was determined by the finely-collimated horizontal X-ray beam. The calculation and resultant graph of cumulative percent versus phi distribution utilize the principle of Stokes' Law. The mean phi, standard deviation, skewness, kurtosis, and normalized kurtosis were calculated according to Folk and Ward (1957).

#### Clay Fabric Preparation Techniques

The techniques used for sample preparation of the pelagic clay sediments for fabric studies using transmission electron microscopy (TEM) and scanning electron microscopy (SEM) follow procedures described by Bennett (1976), Bennett et al. (1977), and Bennett and Hulbert (1986). The techniques are outlined below. Sample preparation and dehydration techniques common to TEM and SEM are

- Subsampling of sediment from cores

- Replacement of saline interstitial water by a series of miscible fluids (ethyl alcohol-amyl acetate) (complete removal checked by precipitation of silver chloride)
- Careful wrapping of small specimens in thin lens paper
- Further soaking of specimens in amyl acetate
- Placement of specimens in the critical point chamber
- Purging of specimens, with liquid CO<sub>2</sub> replacing amyl acetate
- Critical point drying with CO<sub>2</sub> (see discussion of technique below)
- Placement of dried, wrapped specimens in small individual desiccators.

Additional sample preparation techniques specific to TEM are

- Placement of individual specimens (wrapping paper removed) in small containers, followed by placement in a large desiccator under vacuum
- Impregnation of individual specimens under vacuum with very low viscosity Spurr epoxy resin
- Removal of specimens from the vacuum and subsequent curing of the epoxy resin at 60 to 70°C
- Trimming of the specimens with glass knives prior to ultra-thin sectioning (larger specimens were trimmed beforehand with a jeweler's saw)
- Ultra-thin sectioning with a diamond knife (sections cut approximately  $5 \times 10^{-8}$  to  $1 \times 10^{-7}$  m thick [-500 to 1000 Å]) on a microtome
- Placement of ultra-thin sections on copper grids
- Very light carbon "sputtering" of ultra-thin sections and grids in a vacuum evaporator
- Examination of the clay fabric of the specimen.

Additional sample preparation techniques specific to SEM are

- Making a shallow incision with a razor blade to fracture the sample, exposing fresh surfaces
- Mounting the sample on an aluminum stub with double-stick tape or other adhesive
- Cleaning the exposed sample surface with an electrostatic field created by rubbing a cellulose-acetate-butyrate plastic tube with a lint-free cloth and passing it over the sample, which discharges the mounting stub
- Heavy "sputtering" of the mounted sample with palladium/gold wire in a vacuum evaporator
- Examination of the surface features.

#### Critical Point Drying

The interstitial water (34.2 ‰ salinity) of the saturated sediment samples was slowly replaced by serial increases of absolute ethanol (1:5, 2:5, 3:5, 4:5, 1:1). The serial exchange is performed to minimize change in the dielectric constant of the intermediate fluids and provide a more gentle chemical treatment of the fabric samples. Complete removal of the Na<sup>+</sup> and Cl<sup>-</sup> ions in the pore water was verified by the silver nitrate test (Bennett et al., 1977). A white precipitate is indicative of residual Cl<sup>-</sup> ions in the pore fluid. The samples were sectioned with a razor blade into blocks of about 0.5 cm and wrapped in lens paper, which was gently folded and clipped to form small protected packets. These packets were soaked in amyl acetate, and liquid CO<sub>2</sub> was used in the critical point drying process. Several packets per run were dried in a Denton DCP critical point drying apparatus.

The critical point technique is a marked improvement over other dehydration methods because surface tension forces are avoided (Bennett and Hulbert, 1986). At the critical temperature and pressure of a liquid, no boundary exists between the liquid and gas phase; when the temperature is held above the critical point, the gas may be released until atmospheric pressure is reached. Thus, the sample can be dried without surface tension effects that are extremely deleterious to clay fabric. Intermediate fluids such as acetone, alcohol, and amyl acetate are often used as transition media because it is usually necessary to interpose one of these liquids between the aqueous phase of the sample and the liquid CO<sub>2</sub> or other critical point fluid. The critical point fluid is introduced into the sample chamber "bomb" in the critical point apparatus, and the specimen is purged until the intermediate fluid is removed. The sample chamber is closed at the purge valve and then raised to a pressure above the critical point of the fluid for drying. The critical point for liquid CO<sub>2</sub> is reached at 1125 lb/in.<sup>2</sup>, held for approximately 30 minutes, and finally degassed slowly by opening the purge valve.

#### Embedding

Great care was taken in unwrapping the packets and placing the samples in Beam capsules containing a small amount of Spurr epoxy resin. The capsules were then filled with Spurr resin, which increased impregnation efficiency because of its very low viscosity (60 centipoise) compared to other widely-used, high-viscosity (~2,000 centipoise) epoxies. The reagents of Spurr for a hard cure, by weight, are

- Vinyl cyclohexene dioxide (5 g)
- Nonenylsuccinic anhydride (13 g)
- Diglycidyl ether of polypropylene glycol (3.5 g)
- Dimethyl amino ethanol (0.2 g).

A vacuum was applied to the samples to aid the impregnation of resin into the samples. During the embedding process, it was determined that samples originally having a high water content (low cohesive strength) remained intact if impregnated under a vacuum. Samples having a very complex fabric retained their particle-to-particle structural integrity. The capsules were heated in a 70°C oven for 24 hours to polymerize the resin into a very hard plastic. Samples were hand trimmed using a razor blade to carve a trapezoid approximately 1 mm in length and 0.5 mm in height on the face of the area selected for microtoming. Using a Sorvall Porter-Blum Ultramicrotome MT-2, sections were cut to a thickness of approximately 800 Å, as determined by optical properties (gold-colored). These sections were clustered on the water surface, mounted on a #200 mesh copper grid, and carbon coated for stability while in the electron microscope. The specimen was then ready for examination using TEM. A Zeiss 10 electron microscope was used at 60 kv. Micrographs were taken at magnifications of 8000x and 16000x.

#### Rose Diagram

Fabric orientation analysis was performed on samples B-4 and B-5 from core PC-2, sample B-7 from core PC-1, and RAMA representative single micrographs (Figures 6[c], 7[c], 8[c], and 9[c]). A RAMA mosaic of 20 micrographs, photographed within one grid square, was also analyzed (Figure 10). The direction of elongation of the particles and domains was measured from the micrographs in reference to an arbitrary straight line. Approximately 200 grains were measured and recorded in 10-degree increments from 0 to 1800 degrees on the single micrographs. The particles measured on the mosaic were categorized by size. More than 100 particles and small domains ranging in size from 0.2 to 0.5 μm were examined. Also, more than 300 domains from

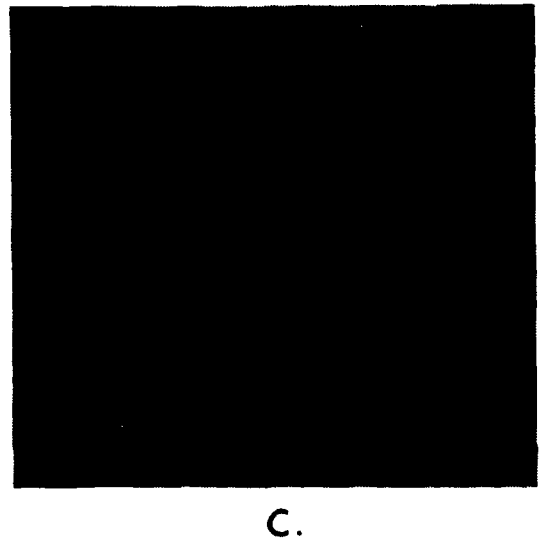
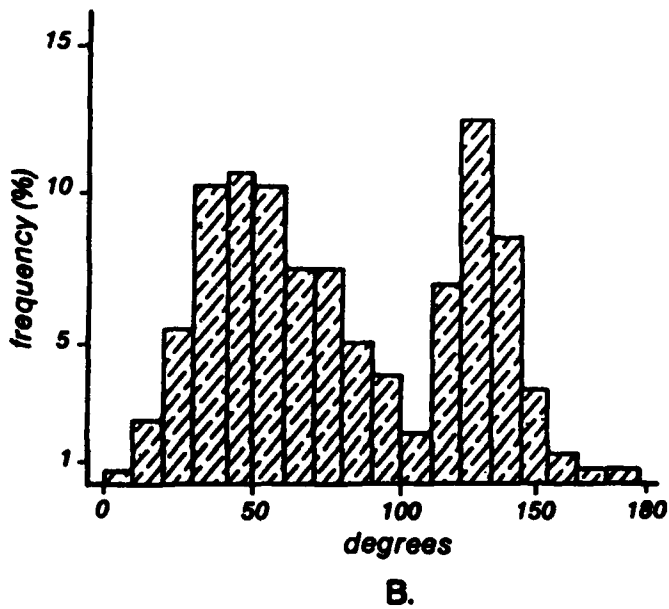
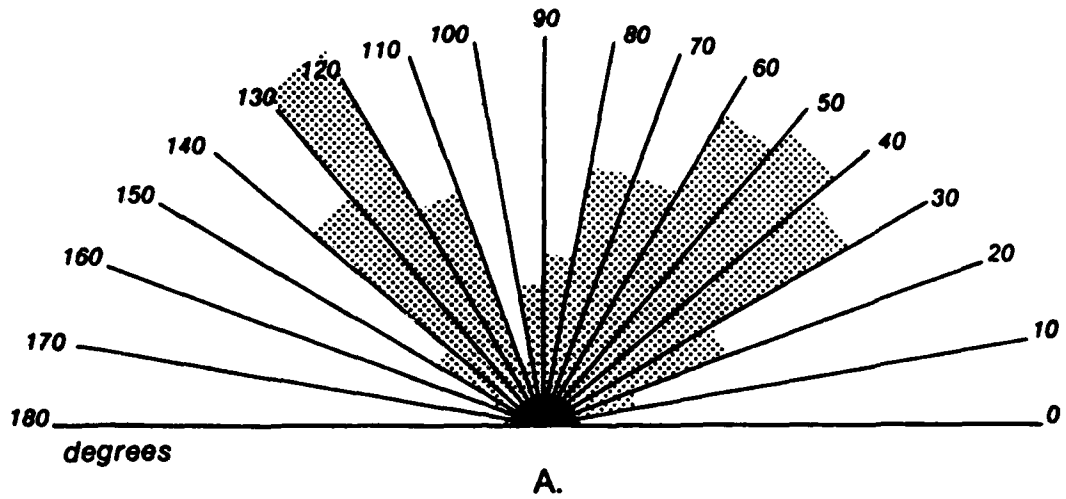


Figure 6. Sample B-4: Rose Diagram (A), Frequency Histogram (B), and TEM Micrograph (C) (Bar Scale = 1  $\mu\text{m}$ ) Showing Biomodal Distribution of Particles.

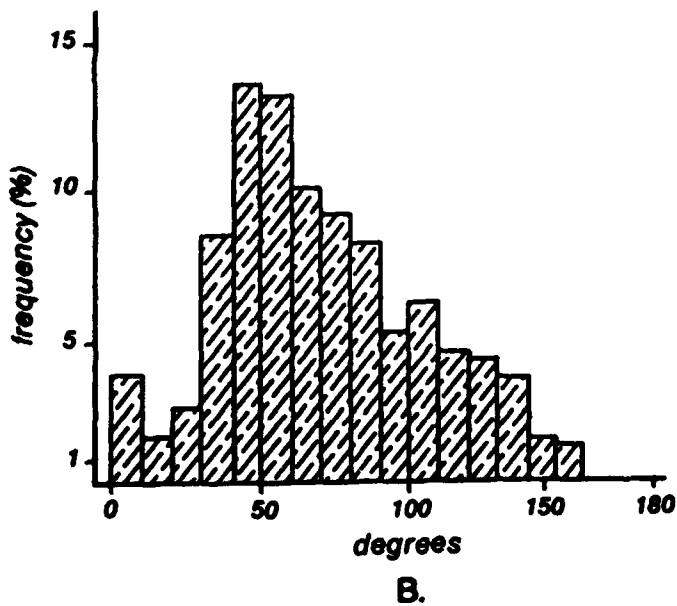
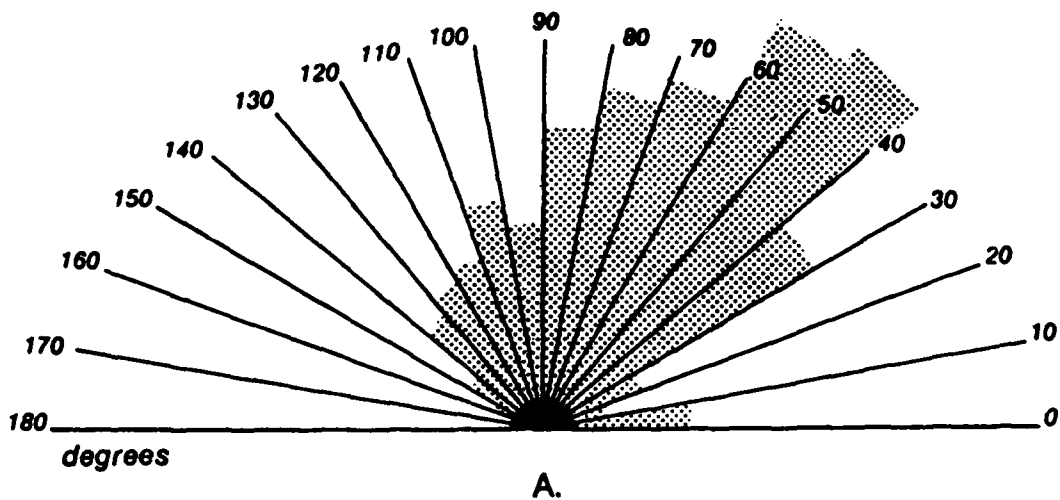


Figure 7. Sample B-5: Rose Diagram (A), Frequency Histogram (B), and TEM Micrograph (C) (Bar Scale = 1  $\mu\text{m}$ ) Showing Some Preferred Particle Orientations Similar to a Normal Gaussian Distribution.

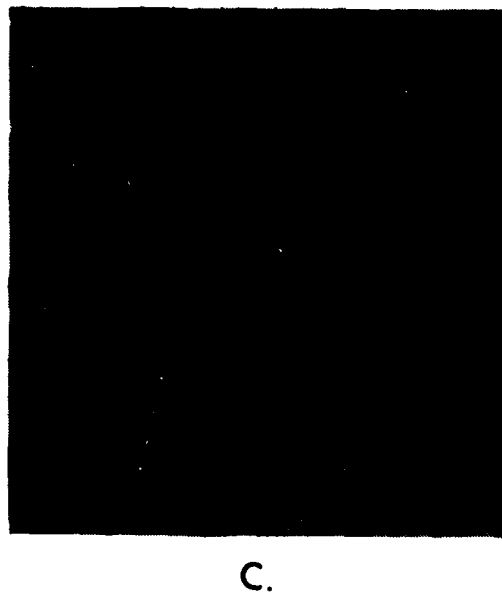
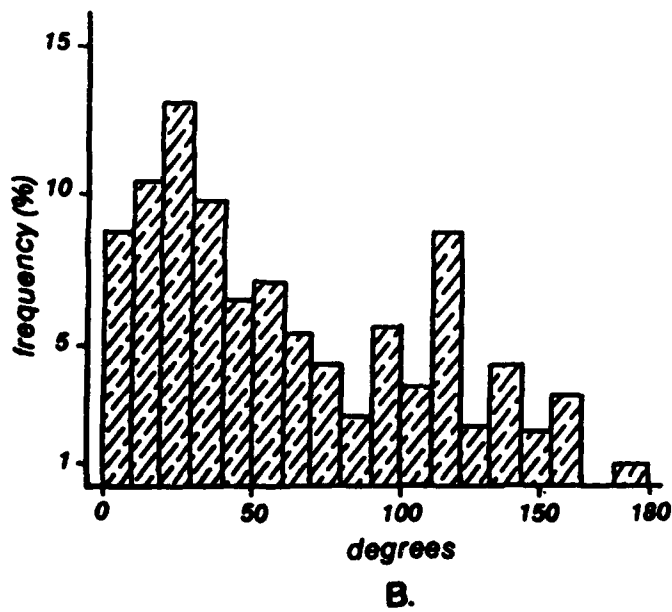
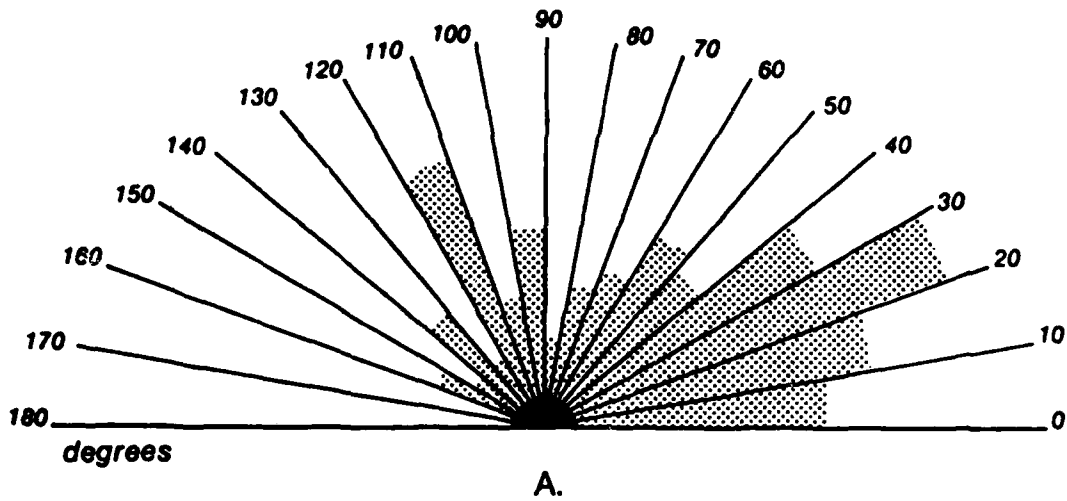


Figure 8. Sample B-7: Rose Diagram (A), Frequency Histogram (B), and TEM Micrograph (C) (Bar Scale = 1  $\mu\text{m}$ ) Showing a Slightly Bimodal Distribution of Particles.

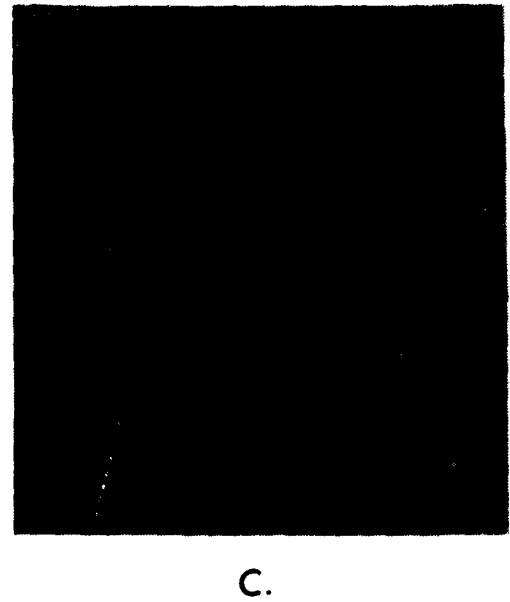
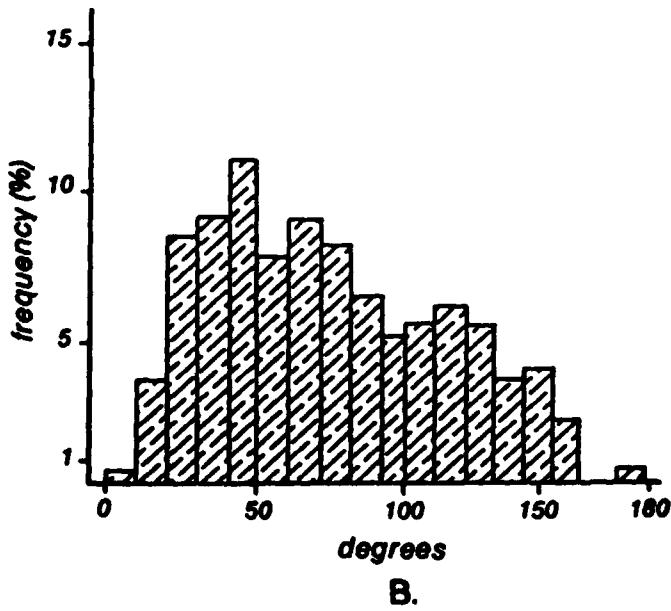
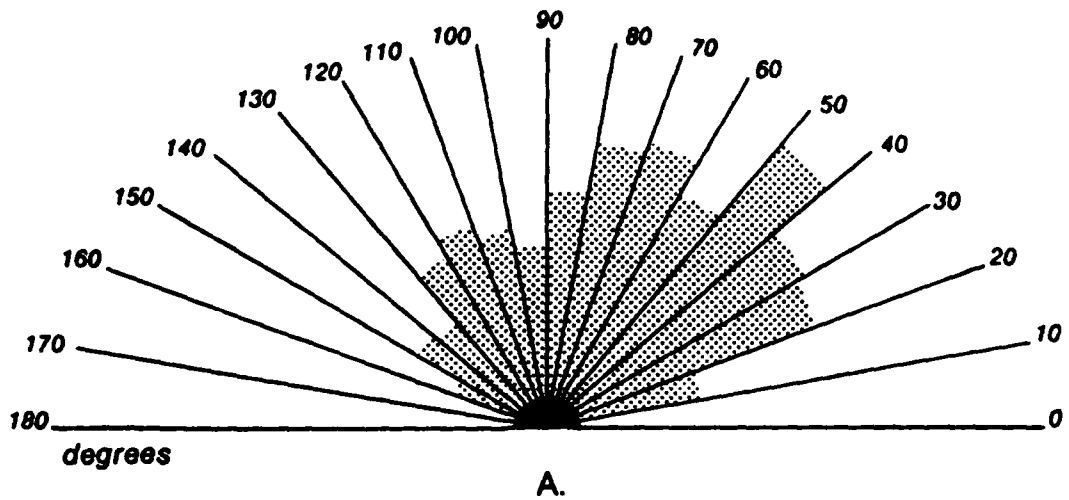


Figure 9. RAMA Sample: Rose Diagram (A), Frequency Histogram (B), and TEM Micrograph (C) (Bar Scale = 1  $\mu\text{m}$ ) Showing a Slight Particle Orientation Preference.





Figure 10. RAMA Mosaic.

1 to 5  $\mu$ m were measured when an obvious elongation could be determined. The micrographs used for this analysis were enlarged 18,000 times, and the mosaic was enlarged 10,000 times. The resulting plot from the measured orientations, the rose diagram, and frequency histogram (Figures 6[a and b], 7[a and b], 8[a and b], 9[a and b], and 11) provide a data base for comparison between samples. The frequency histogram was derived by calculating the percentage of particles in each 10- $\mu$  increment from the total count and plotting frequency (%) versus degrees.

#### X-Ray Diffraction

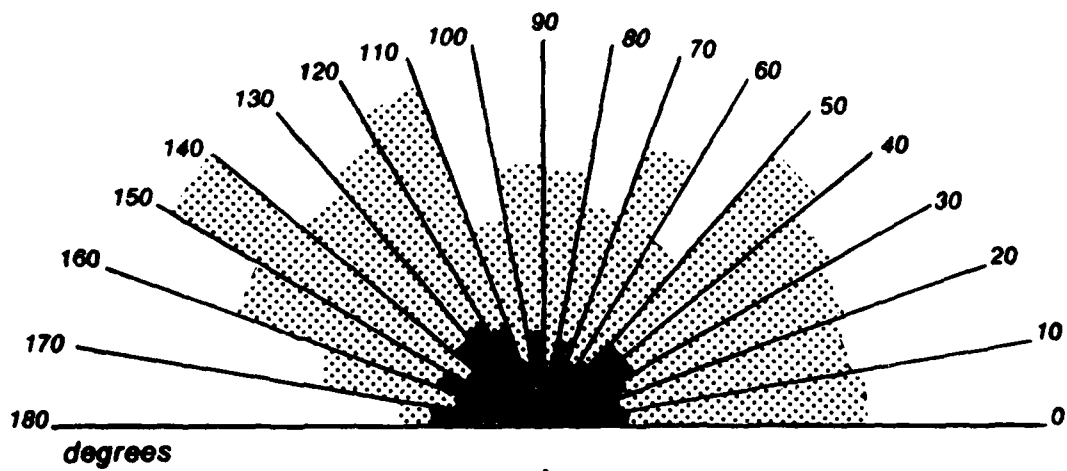
X-ray diffraction was performed using techniques modified from Jackson (1969). Carbonates, organic matter, manganese dioxide, and free iron were removed. This was necessary because they act as binding agents and inhibit dispersion, interfering with fractionation and particle size determination. Fractionation was accomplished by optimizing the pH, centrifuging with pH 10  $\text{Na}_2\text{CO}_3$ , and flocculating in 1 N  $\text{NaCl}$ . The samples were saturated with magnesium and potassium. X-ray diffraction patterns of clay minerals, particularly those of expandable layer silicates such as smectite, are affected by the cation saturating the exchange sites. Other relevant factors include the kind and amount of solvating liquid, and temperature of samples when X-rayed. Diagnosis of clay minerals present is determined by the extent of swelling along the "c" crystallographic axis when cation saturated, and contraction or shrinkage when heated at different temperatures. Oriented specimens were prepared by air drying a slurry of the clay on a glass slide. Vicor glass was used for the heated samples. The  $\text{Mg}^{++}$  saturated samples were X-rayed at 25°C (room temperature), glycerol solvated, and X-rayed again. The  $\text{K}^+$  saturated sample slide was X-rayed following heat treatment at 25, 330, and 550°C.

## RESULTS AND DISCUSSION

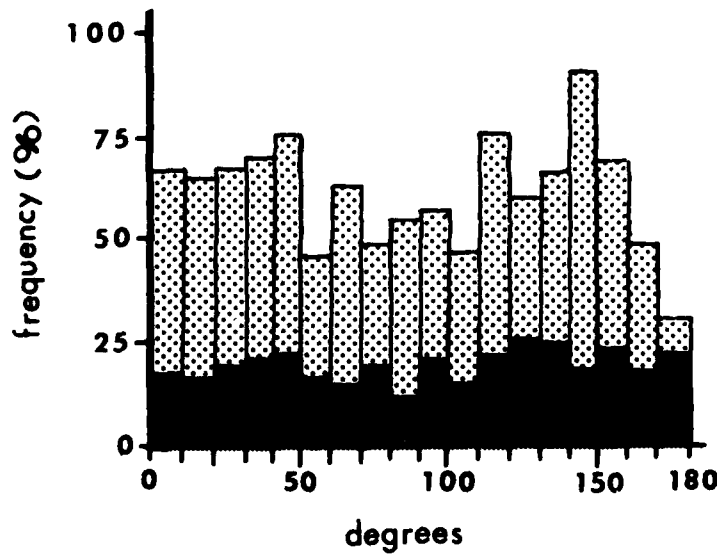
### Thermal Effects

The steady-state isotherm diagram (Figure 12) shows fabric sample locations and the thermal fields generated by the heater probe for a total power dissipation of 160 watts. The highest temperature generated, 296°C, occurred in a narrow region surrounding the lower 15 cm of the heater probe. Fabric sample B-8 was located in the highest-intensity thermal zone, 100-296°C. Rapid decreases in temperature were recorded radially away from the heater. Fabric samples B-1, B-3, B-7, and B-9 fell within the 100-200°C isotherm gradient. Samples B-2, B-6, and B-10 were located proximal to the 100°C isotherm. Fabric samples B-4, B-5, B-11, and B-12 were exposed to temperatures within the 50-100°C zone.

The water content (expressed as percent dry weight) of the sediment from the cusp between cores PC-1, PC-2, and PC-3 (Figure 4) varied with sediment depth. Figure 13 illustrates the 10% reduction (102 to 92%) in water content from 8 to 33 cm below the sediment surface (mudline). Beyond the end of the probe at 33 cm, the water content increased slightly less than 10%, which is close to the value at 8 cm. Figure 14 is a composite plot from cores PC-1 and PC-2 showing the water content change radially from the heater at 24.6 to 28.2 cm below the mudline. The water content decreased from the maximum value of 115.6% at 1 cm from the sediment-heater interface to a minimum of 90.6% at 3.2 cm; a 21.6% reduction in moisture content occurred radially in only 2.2 cm. Baking in the ISIMU experiment (assuming 100% saturation of the sediment) was followed by consolidation of sediments and loss of pore fluid. This was conspicuous in the 19% decrease in void ratio from 3.1 to 2.5. Radially from the heater, water contents were low (between



A.



B.

Figure 11. Rose Diagram (A) and Frequency Histogram (B) for RAMA Mosaic (Figure 10) Showing a Completely Random Distribution of Particle Arrangements. The dark areas represent 2-5  $\mu\text{m}$  domains, and the lighter areas represent  $\leq 1 \mu\text{m}$  small particles and domains.

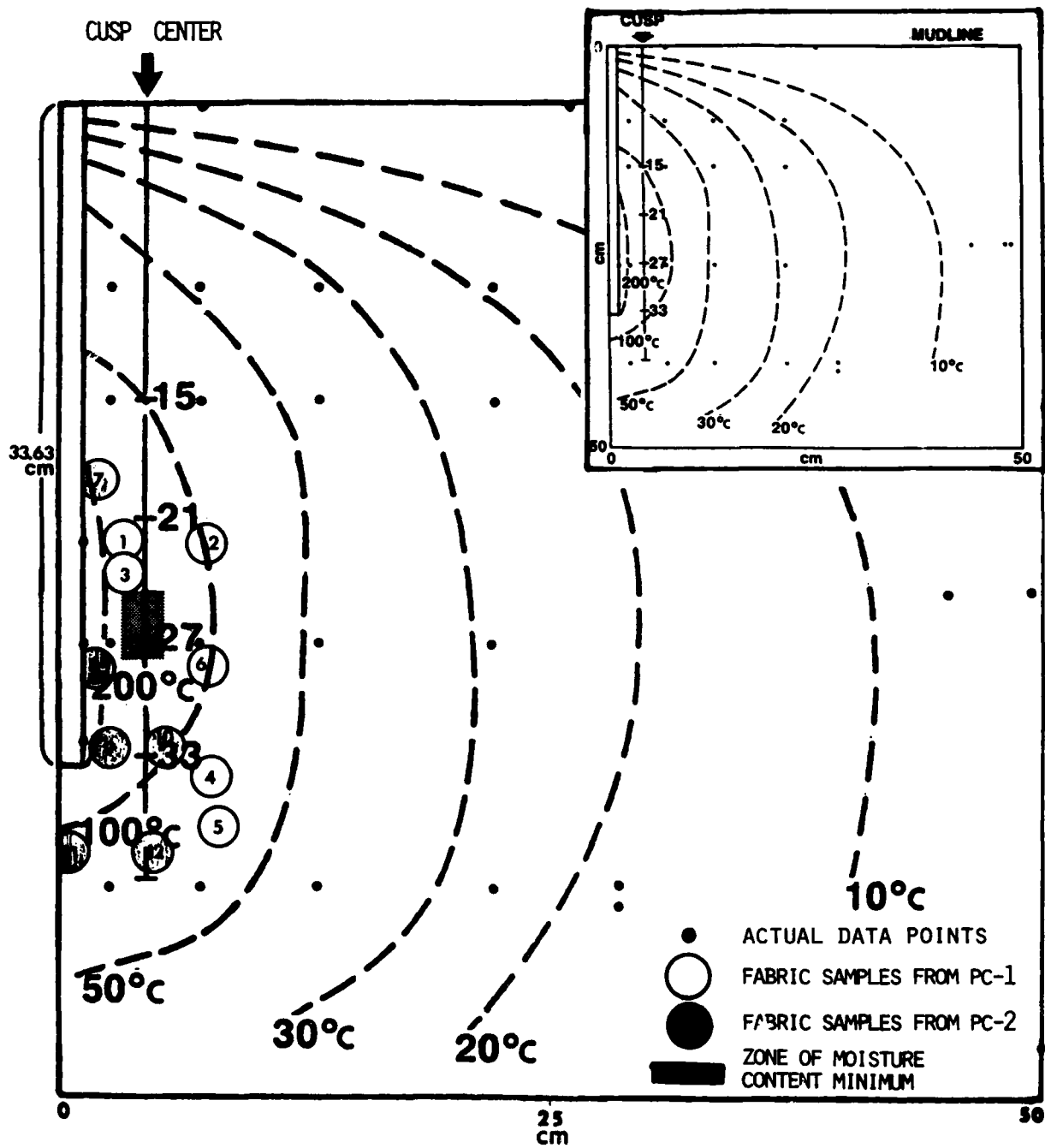


Figure 12. Steady-State Isotherm Showing Position of 12 Fabric Samples, and the Cusp Samples Used for X-ray Diffraction Analysis (Drafted by H. Li, Extrapolated from Experimental Data, Miller et al., 1982).

2 and 4.7 cm), which includes the cusp zone created between cores 1, 2, and 3. Beyond approximately 5 cm, the water content fluctuated. The grided areas of Figures 12, 13, and 14 represent the zone of minimum water. No fabric samples were collected from this zone, but assuming axial symmetry of the thermal gradients (100-200°C), sediment of samples B-1, B-3, B-9, and B-10 probably experienced the same thermal effects from heating as the grided zone. The significant decrease in water content near the heat source may have resulted from induced thermal effects, resulting in pore water diffusion, consolidation, and chemical reaction.

Thermal heating effects on the orientation of particles were studied by examining the micrographs of samples B-4, B-5, and B-7 in comparison with the RAMA samples. Sample B-7 from core PC-1, adjacent to the heater probe, received the most intense heat and represents a near-field sample (Table 1 and Figure 12). Sample B-4 from core PC-2 was 5.5 cm from the heater's edge; far-field sample B-5, also in PC-2, was 6.0 cm from the probe. Sample B-7 was closest to the mudline at 18.9 cm. Sample B-3 was obtained from a depth of 23.9 cm below the mudline. Sample B-5 was obtained at a sediment depth of 35.9 cm. Samples B-4 and B-5 were within the 50-100°C isotherm gradient, and sample B-7 was within the 200°C boundary. Because the RAMA sample was not subjected to the heat source, its ambient in situ temperature would have been approximately 4°C.

The undrained shear strength profiles are depicted for three vertical test sequences: pretest unheated and heated, and post-test cooled conditions (Silva, 1983 and Figure 15). The large shear strength increase between 20- and 32-cm sediment depth during heating corresponds directly to the water content decrease (Figure 13). The 38-kPa (375 g/cm<sup>2</sup>) shear strength maximum occurring at 170°C corresponds to the 33-cm depth at the end of the heater probe and

probably results from localized dewatering due to heating. The comparison of the maximum shear strength profile during heating and the profile obtained before heating indicate a ten-fold increase in shear strength. At termination of the test (after cool-down), the sediment shear strength appears to have decreased, but not back to its original pretest strengths. This implies a slight, thermally-reversible or residual characteristic strength following cool-down of this sediment type.

#### Mechanical Disturbance

Mechanical disturbance of the sediment includes effects from probe insertion and remolding. Remolding can be considered in terms of primary remolding during preparation of the red clay sediment before emplacement in the ISIMU test tank (Figure 3), and secondary or localized remolding from heater probe penetration into the prepared consolidated sediment. Clay fabric disturbance resulting from probe insertion is difficult to assess using TEM micrographs. When selecting fabric subsamples, extreme care was taken to avoid any obvious pre-existing physical disturbances such as fractures or micro-cracks in the sediment. The penetration stresses from probe insertion are a function of sediment type, velocity of insertion, radius of probe, tip shape, and angle. The largest change in force per unit length of probe displacement ( $\Delta F/\Delta L$ ) occurs as the tip of the probe comes in contact with and begins initial vertical displacement of the surface sediment (Silva et al., 1983). The forces ( $\Delta F/\Delta L$ ) become approximately constant as the sediment contacts the side of the probe. As the probe is inserted deeper into the sediment, the total forces gradually increase in a nearly linear fashion as a result of traction (adhesion) stresses at the sediment/heater wall interface. The fabric samples were collected near the end of the probe at depths of -21 to -38 cm; therefore, surface effects of

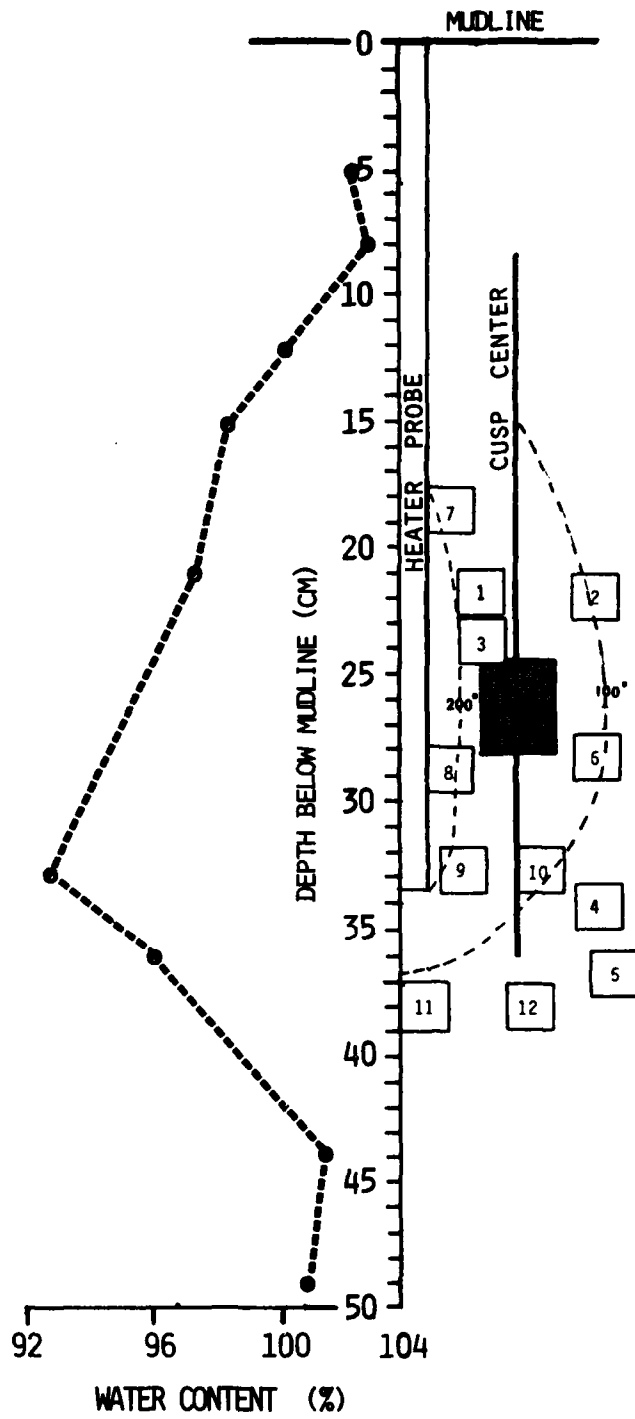


Figure 13. Water Content Versus Depth (cm) Profile for ISIMU Post-Test Samples Showing Water Content Minimum Corresponding to the End of the Heater Probe.

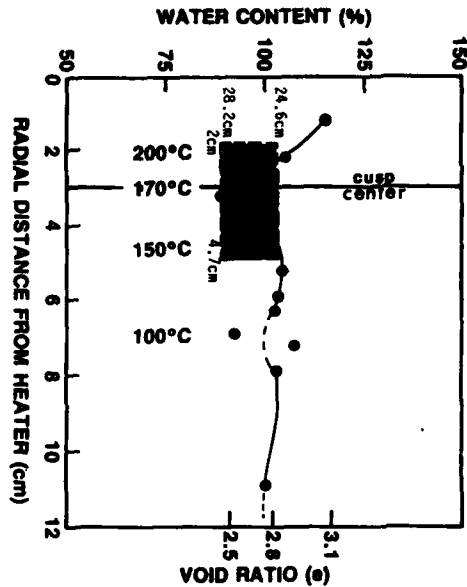


Figure 14. Water Content Versus Distance from the Inconel Heat Source at a Depth of 24.6-28.8 cm. Shaded area denotes zone of lowest water content resulting from heating (modified from Silva, 1983).

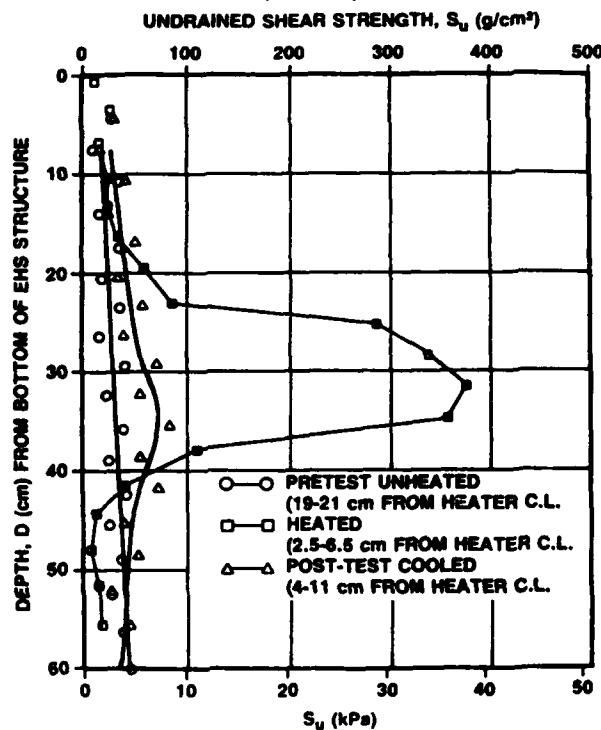


Figure 15. ISHTE Simulation Combined Profile. Note the substantial increase in shear strength associated with the heated zone (redrafted from Silva, 1983).

insertion are not considered. Little difference in traction stresses upon probe insertion were found with varying textures (0.13-2.16  $\mu\text{m}$ ) of the inconel probe's surface (Silva et al., 1983). A 2- $\mu\text{m}$  surface texture finish for the inconel probe was chosen to provide good adhesion (forming a good seal) between the heater and remolded sediment, preventing water migration along the heater wall. After the ISIMU, the heater was overcored, the core liner cut, and the sediment sliced normal to the probe for sampling. If the probe had been extracted, suction forces might have been sufficient to result in large localized sediment deformation. Only fabric samples B-7 and B-8, adjacent to the probe, were expected to show any effect from traction forces during insertion.

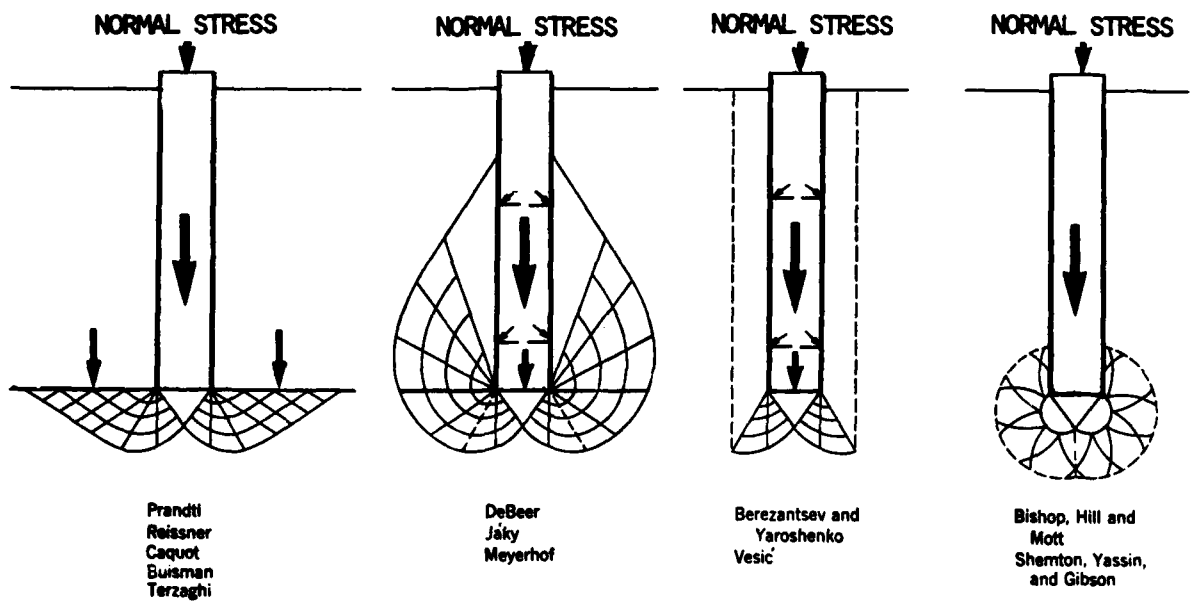
In the process of pile driving and probe/pile insertion in sediments, a recognizable characteristic of soil behavior is a plastic zone of deformation, beyond which is an elastic zone (Figure 16[b]) radiating axisymmetrically from the pile (Randolph, 1978). Plastic deformation is a permanent change of volume shape without rupture, commonly accommodated by grain-grain "gliding." Elastic deformation is a temporary change which disappears when the deforming forces are removed (Bates and Jackson, 1980). The extent of the plastic zone, or yield limit (R) can be calculated theoretically, using

$$R = r_0 (G/S_u)^{1/2}$$

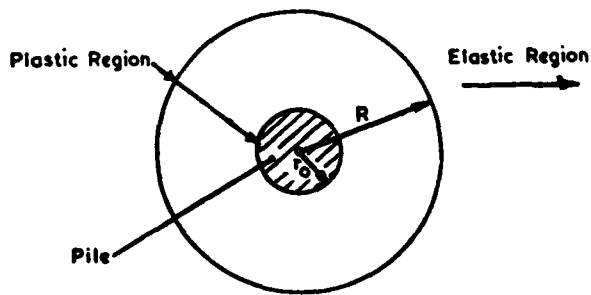
where

- $r_0$  - radius of the heater probe (1.18 cm)
- G - shear modulus of the sediment
- $S_u$  - undrained shear strength (Jordan, 1982).

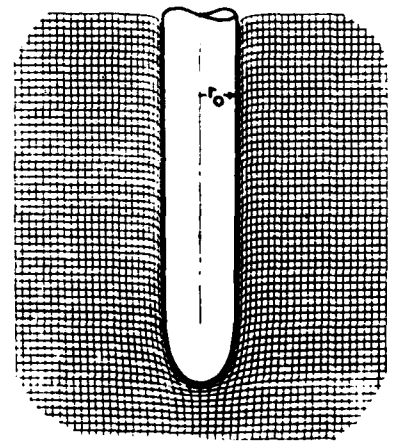
Bennett et al. (1986) calculated  $G/S_u$  values of 18.5 from near-field piezometer data and 132 for far-field data, resulting in R values of 5.1 and 13.6 cm, respectively. Silva et al. (1983) calculated a similar R value of 4.6 from the  $G/S_u$  value of 15.3. The



A



B



C

Figure 16. A) Models of Complex Soil Disturbance Patterns Resulting from Pile Insertion (Modified from Lambe, 1969).  
 B) Zones of Plastic and Elastic Deformation Resulting from Pile Insertion (Redrafted from Randolph, 1978).  
 C) Deformation Patterns Resulting from "Simple Pile" Penetration (Modified from Baligh, 1985).

calculated values of approximately 5 cm for the plastic region (Figure 16[b]) seem more realistic and include all samples except B-2, B-4, B-5, and B-6. Therefore, the micrographs of eight samples within the plastic zone were closely examined for signs of permanent disturbance from probe insertion. Samples B-7 and B-8 are closest to the heater wall (Figure 5) and generally would exhibit the most obvious signs of deformation from probe insertion. The fabric subsamples were extracted from the central portion of the larger samples, and those samples in the plastic zone generally would have characteristics such as smearing of the probe-sediment interface and possibly some lateral deformation from probe insertion.

Figure 16(a and b) shows various theoretical complex disturbance patterns due to the installation of a pile whose length is much greater than its diameter (Lambe and Whitman, 1969). Although these patterns are probably generalized exaggerations of the effect of heater probe insertion, consideration of disturbance effects must be reconciled when examining the TEM micrographs. Samples directly beneath the probe or proximal to the probe's end were probably affected by secondary remolding from probe insertion. Figure 16(c) is a representation of the vertical deformation pattern occurring during penetration of a "simple pile" probably closely resembling the inconel, rounded-end, ISIMU heater probe evenly pushed into a saturated clay sediment (Baligh, 1985). The deformation zone appears to affect only a relatively thin skin of clay adjacent to the heater wall. Baligh's strain path model simplistically considers a uniform velocity field, involving no distortions or strains, on a single source penetrating an incompressible, homogeneous, isotropic clay subjected to an isotropic state of stress, ignoring boundary conditions.

Primary remolding from mechanical disturbance occurred as the illitic-

rich dredged sediment was reconstituted and then churned in a cement mixer before consolidation to in situ overburden pressures. The expected results from remolding were breakage, swirling, or bending of long chains of particles or elongated domains, and collapse and breakage of fragile flocs and aggregates. These effects were expected to be more pronounced on longer particles than on individual particles or subrounded dense aggregates. If significant, primary remolding effects were expected to be evident in all cores, despite their locations in reference to the heat source.

#### Grain Size Analysis

Grain size analysis was performed on two samples. A RAMA sample represented the control and core PC-5 was used to assess the effects of reconstituting and laboratory remolding of sediment for experimental purposes. Core PC-5 represented a far-field sample, and was located well beyond effects from intense heat, such as decrease in water content or increase in shear strength. The grain size analysis shows a striking similarity between the two samples (Figure 17). They were both extremely homogeneous with only trace amounts of sand (greater than 4 phi). The predominant particles were clay-size ( $\leq 3.9 \mu\text{m}$ ) and comprised ~90% of the sample. The silt content of both samples was ~10%, and the remaining portions were sand. These results imply negligible effects on the clay-size particles from reworking of the illitic-rich pelagic sediment. For all practical purposes the two samples analyzed were identical.

#### X-Ray Mineralogy: Pre- and Post-ISIMU

Samples from various depths approximately 3.5 cm from the heater centerline in the cusp between cores PC-1, PC-2, and PC-3 were analyzed for clay mineralogy. At a depth of

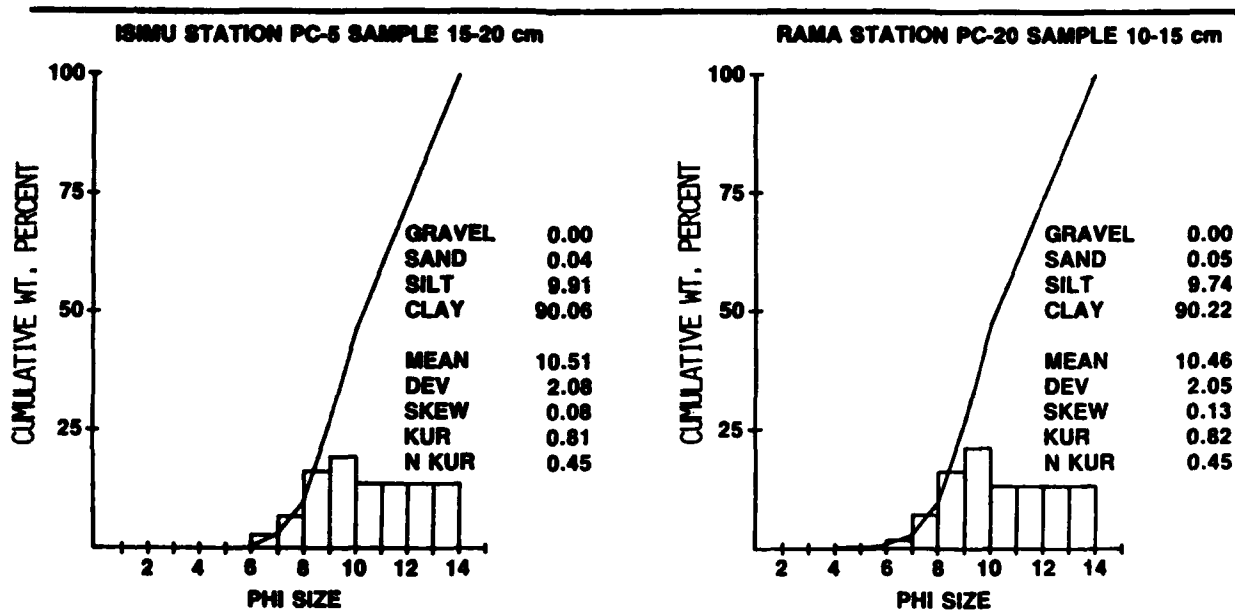


Figure 17. Grain Size Comparison of RAMA Sample to Sample PC-5, Which Was Remolded and Laboratory-Consolidated to Equivalent In Situ Porosity. Notice the striking similarity of the grain sizes.

7 cm, the sediment was composed of approximately 5% smectite, 34% chlorite, 48% illite, and 13% kaolinite. At 24 cm the mineral composition changed to approximately 40% smectite, 20% chlorite, 40% illite, and trace amounts (less than 5%) of kaolinite. After consideration of the limits of instrument detection (at least 5% of a mineral in question is necessary for confirmation) and possible errors in calculations, a significant smectite increase accompanied by a change in color from brown to grey is evident. The 7-cm depth is associated with a thermal gradient between 50-100°C and water content of 103% (Figures 12 and 13). At 24 cm the temperature recorded during the experiment increased to 170°C, with an associated post-test water content of 97%. The water content is a measure of the intergranular pore water and free water or interlayer water not strongly attracted to the mineral skeleton.

Routine water content determination dries the sample in a 105°C oven. Greater temperatures remove more of the loosely bonded water, although temperatures of approximately 500°C are required to remove the adsorbed water layer of smectite, collapsing its structure. In a closed system, loss of pore water would have to be balanced by incorporation of more water into the interlayers. This would be seen on X-ray patterns as a peak shift to the right (depending on the cation present) from 12 to approximately 18 Å, indicating expansion of the crystal lattice. Increased quantities of smectite are detected by an increase in the peak height on the X-ray patterns. This was evident in the cusp sample at 24 cm (Figure 18). Thornton (1983) studied the transition of a sediment's mineralogy from mixed smectite/illite to an increase in smectite and decrease in mixed-layer clays, after being maintained in a 200-300°C hydrothermal apparatus. Potassium, the cation

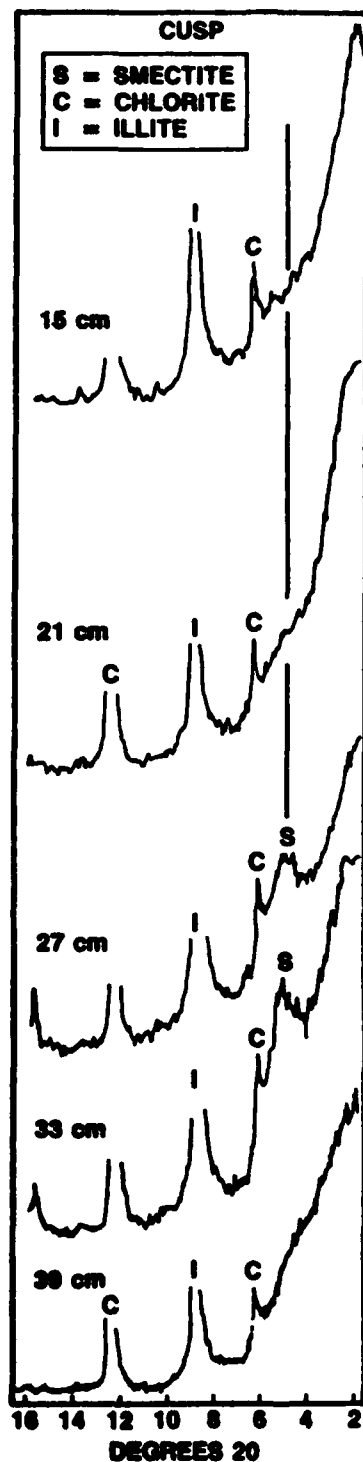


Figure 18. X-ray Diffraction Patterns Showing Pronounced Increase in the Smectite Peak Occurring at the 27- and 33-cm Depths.

associated with illite, binds successive layers. From chemical analysis of the pore fluids, an increase in the potassium level was detected in an area adjacent to the cusp. A thermally-induced release of interstitial potassium may have resulted in the transformation to smectite, although other geochemical processes and minerals may have played a role in smectite formation.

#### Fabric Analysis

Analysis of the single RAMA sample micrographs indicates that some preferred particle alignment occurs. However, analysis of more than 1000 particle measurements on the RAMA mosaic revealed a random arrangement of particles (Figure 10) as seen in the histogram and rose diagram (Figure 11). The near-field micrograph of sample B-7 had a slight bimodal distribution of particle orientations, and sample B-4 showed a similar, but more pronounced bimodal distribution. The angle between the two bimodal planes was approximately 90 degrees in both bimodal samples. Far-field sample B-5 had the strongest degree of preferred orientation, demonstrated by its rose diagram and frequency histogram (Figure 9), but was exposed to the lowest thermal gradient. Thus, particle orientation appears to be independent of sample proximity to the generated thermal gradient determined from orientation analysis. Additional analysis of remolded, nonheated fabric is needed to evaluate the dominant parameter causing particle alignment (heating, remolding, or both). If the remolded samples demonstrate preference of particle alignment, as indicated from the individual micrographs, perhaps the movement of pore fluids could be sufficient to move particles or small domains to a preferred orientation. Consolidation, the decrease in volume of the sediment resulting from loss of pore fluid, is an expected outcome from exposure to increasing temperature. The flow of

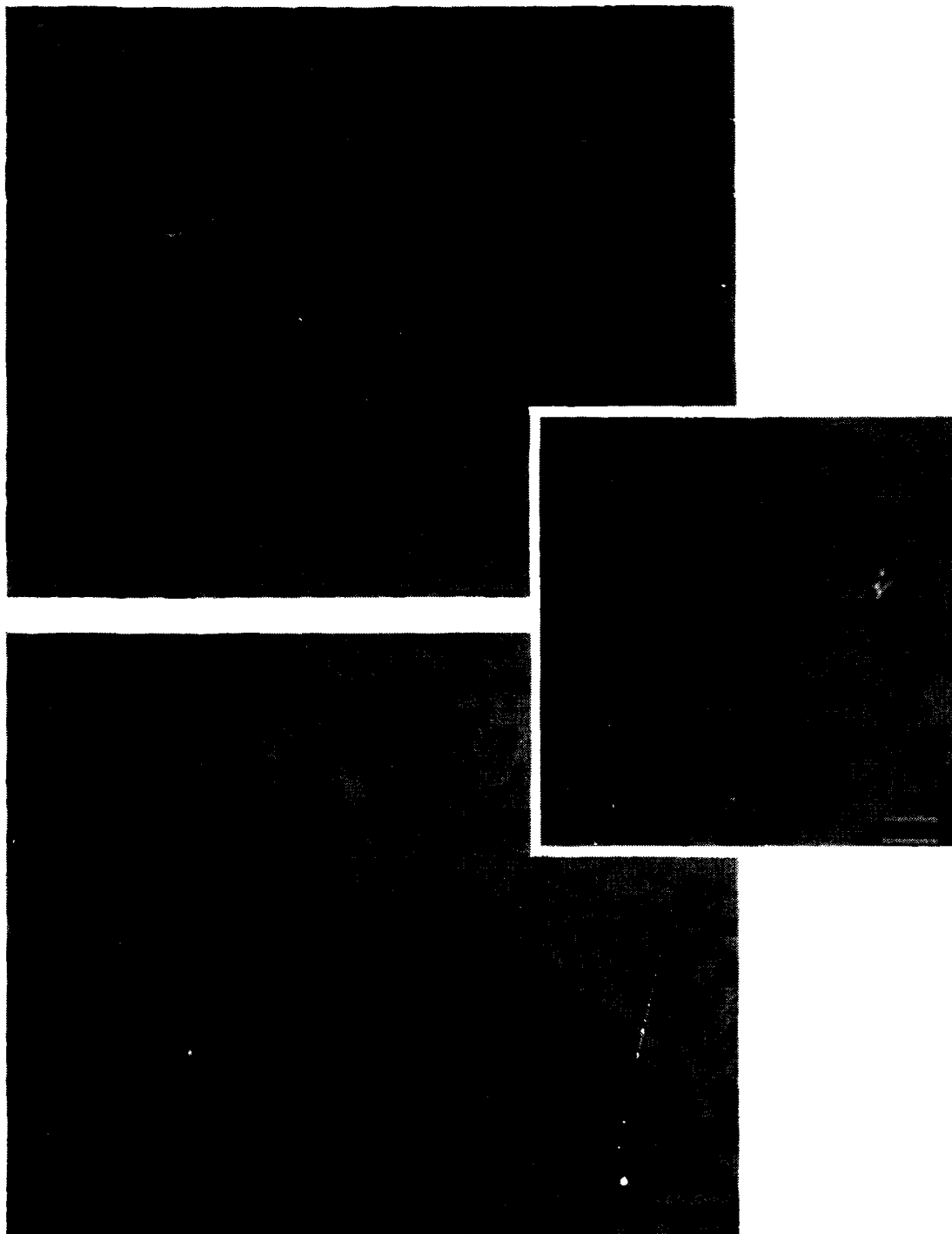
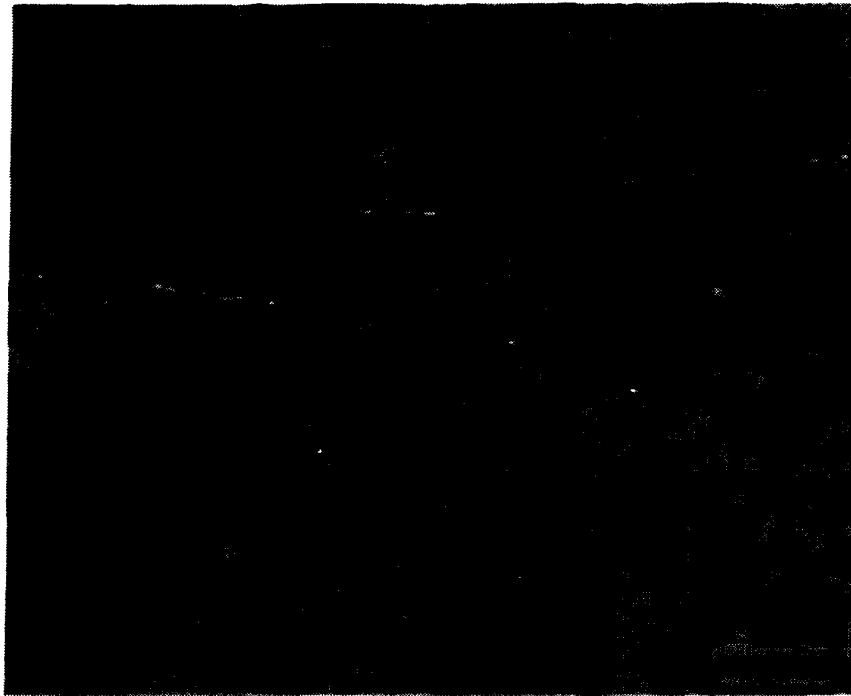


Figure 19. Probe Insertion Disturbance Features: A) Denser Arrangement of Particles Forming Broad Zones Defined by Micro-Shear Planes in the Near-Field Fabric Sample B-8; B) An Enlargement of the Micro-Fracture Showing  $\sim 0.5 \mu\text{m}$  Band of Oriented Small FF Domains; C) A Micro-Fracture Lined by Oriented Domains (Arrows).

1)



2)

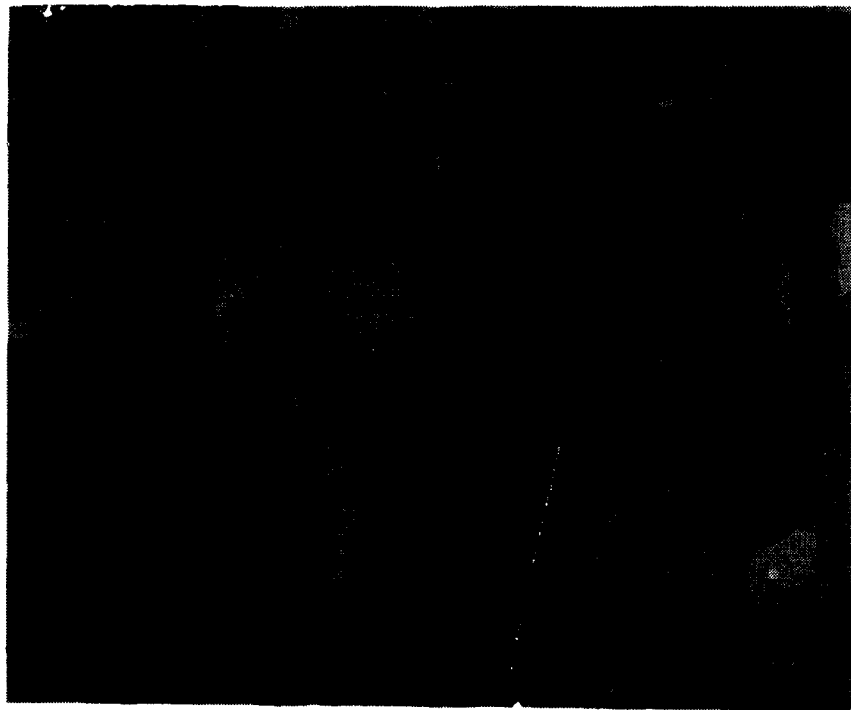


Figure 20. Probe Insertion Disturbance Features: 1) Less Obvious Shear or Micro-Fracture (Dark Lines) Identified by Chains of Stepped FF Small Domains; 2) A More Easily Recognizable Micro-Fault Lined by Oriented Domains. The swirled domains (D) are possibly caused by remolding or shearing adjacent to larger argillites (A). The "fluffy," nonaggregated, fine particles (inside circle) are perhaps authogenic flocculated smectite.

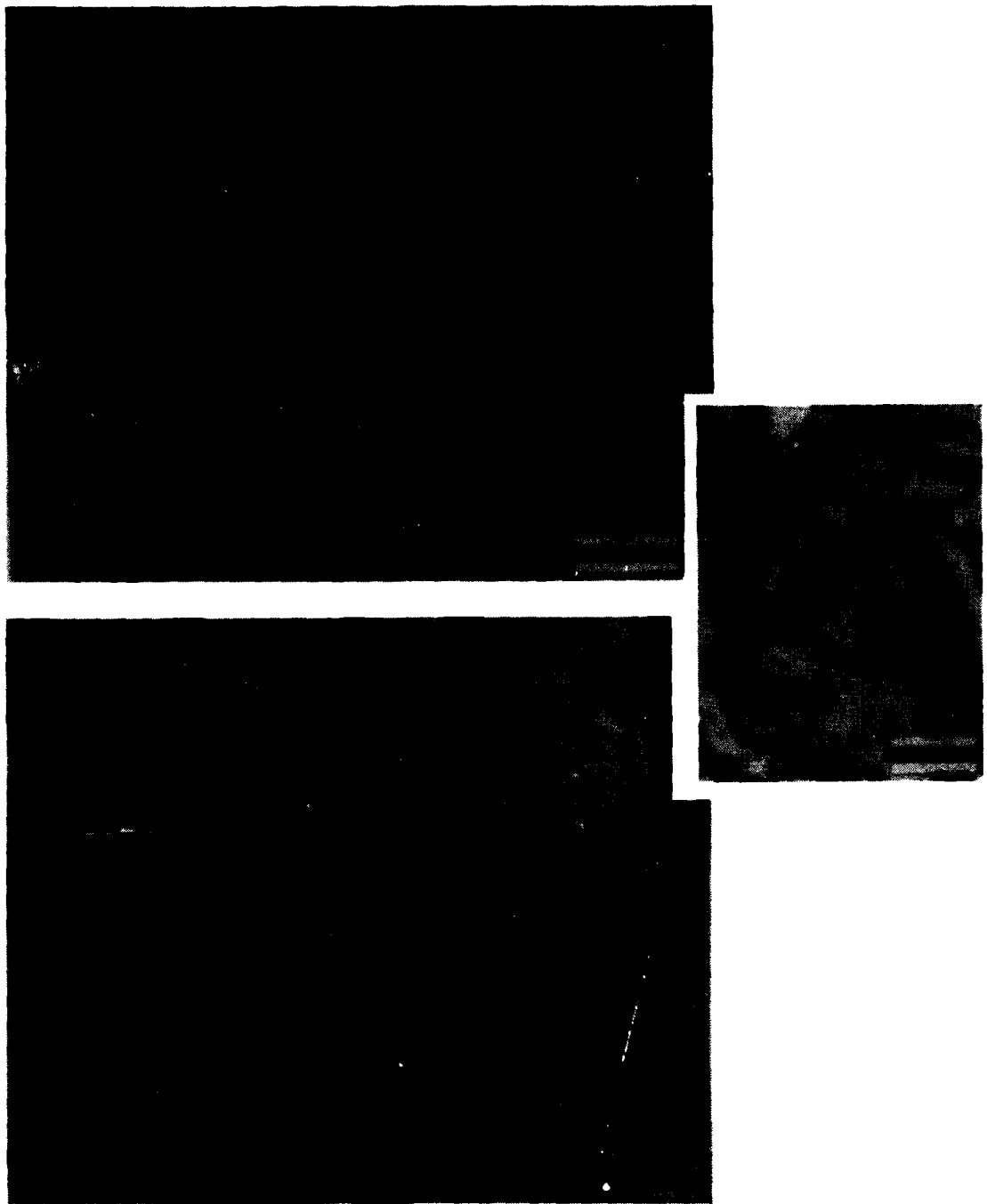


Figure 21. A) Primary Remolding Causing Swirling of Domains (Arrows) and Formation of Voids Performing as Pathways (Dotted Lines) for Pore Fluids and Small Particle Transport; B) Enlargement of Chain of Domains Bent During Remolding; C) the Less-Dense Fabric of a RAMA Sample, Not Subjected to Remolding or Probe Insertion Stress, Demonstrating Characteristic Straight, Long Chains of Domains (Arrow).

water originating in the "baked" zone could have affected the samples in the cooler zones. The processes of consolidation and fluid transport during the ISIMU have been thoroughly documented by Mctigue et al. (1986).

Sediment response to a heat source was evaluated by examining TEM micrographs of the 12 fabric samples from ISIMU cores PC-1 and PC-2. Evidence of disturbance from probe insertion was seen in near-field fabric samples B-7 and B-8, which were adjacent to the heater wall. Sample B-8 shows a slightly denser arrangement of particles than far-field samples such as B-5 (Figure 19[a]). The fabric has the appearance of broad bands between which are long zones of oriented small domains. These appear to be compression features resulting from probe insertion, and look like micro-fractures, or slip or shear planes. Figure 19(b) (sample B-11, located under the probe) is an enlargement of the localized oriented chains, predominately face-to-face, which form a band about 0.5  $\mu\text{m}$  across. Figure 19(c) demonstrates how the shear planes become aligned with chains of oriented domains. The micro-fracture of sample B-8 of Figure 20(a) is subtle because of the lack of separation between the slip planes, but demonstrates the zone of locally oriented particles. Figure 20(b) shows disturbance, evinced by the gap lined with oriented particles. Notice the bent domains, possibly from shearing with planes containing larger, subrounded argillites, resulting in localized or secondary remolding.

A possible diagnostic feature of primary remolding is evident as chains of swirled domains caused by initial mixing of the sediment before emplacement in the pressure tank. An example from sample B-8 (Figure 21[a]) shows chains wrapped around a central group of particles. The voids formed by the swirls seem interconnected and might provide a pathway for movement of pore fluids. Figure 21(b) shows an enlarged swirled or bent domain, which

could be a primary remolding feature. These disturbance features have been observed in other studies (Bohlke and Bennett, 1980; Bennett et al., 1981). Evidence of mixing or stirring is more apparent in long chains, but the dominant particle type in this fabric is short chains. Severe remolding is not as easily observed in the remolded samples. Primary remolding effects are therefore subtle and expected to be present in all the ISIMU samples. Figure 21(c) of the RAMA sample depicts nonremolded, nondisturbed fabric. Notice the straight chain of edge-to-edge small domains not influenced by processes involving remolding or probe insertion.

Although the overall fabric of the near-field samples appears slightly denser than the RAMA sample fabric (Figure 21[b]) as a result of probe insertion, frequent large voids (Figure 22[a-f]) exist, lined with oriented particles and small domains ( $\leq 1 \mu\text{m}$ ) arranged stepped face-to-face and end-to-end. These voids can be thought of as "quasi-expansion" features, and appear to be cross-sections of micro-channels formed by pore fluids moving through the sediment after expansion from thermal forces. Upon heating, the pore fluids may transport the smallest particles, which form the lining of the channels. These conduits are relatively free of small particles, except those too large to be transported, as seen in Figure 22(b-e). The resin-filled voids are not to be confused with the white holes in the ultra-thin sections (Figure 23[a], upper left-hand corner) caused by brittle domains being plucked during microtoming.

An interesting feature more prevalent in the high temperature zones is the appearance of "onion-skin" layering (first described by Brewer, 1964) of stepped face-to-face (Figure 1) of particles surrounding the low density "smectitic" aggregate depicted in Figures 23(a-b) and 24(a-b). Cation exchange capacity (CEC) is the measure

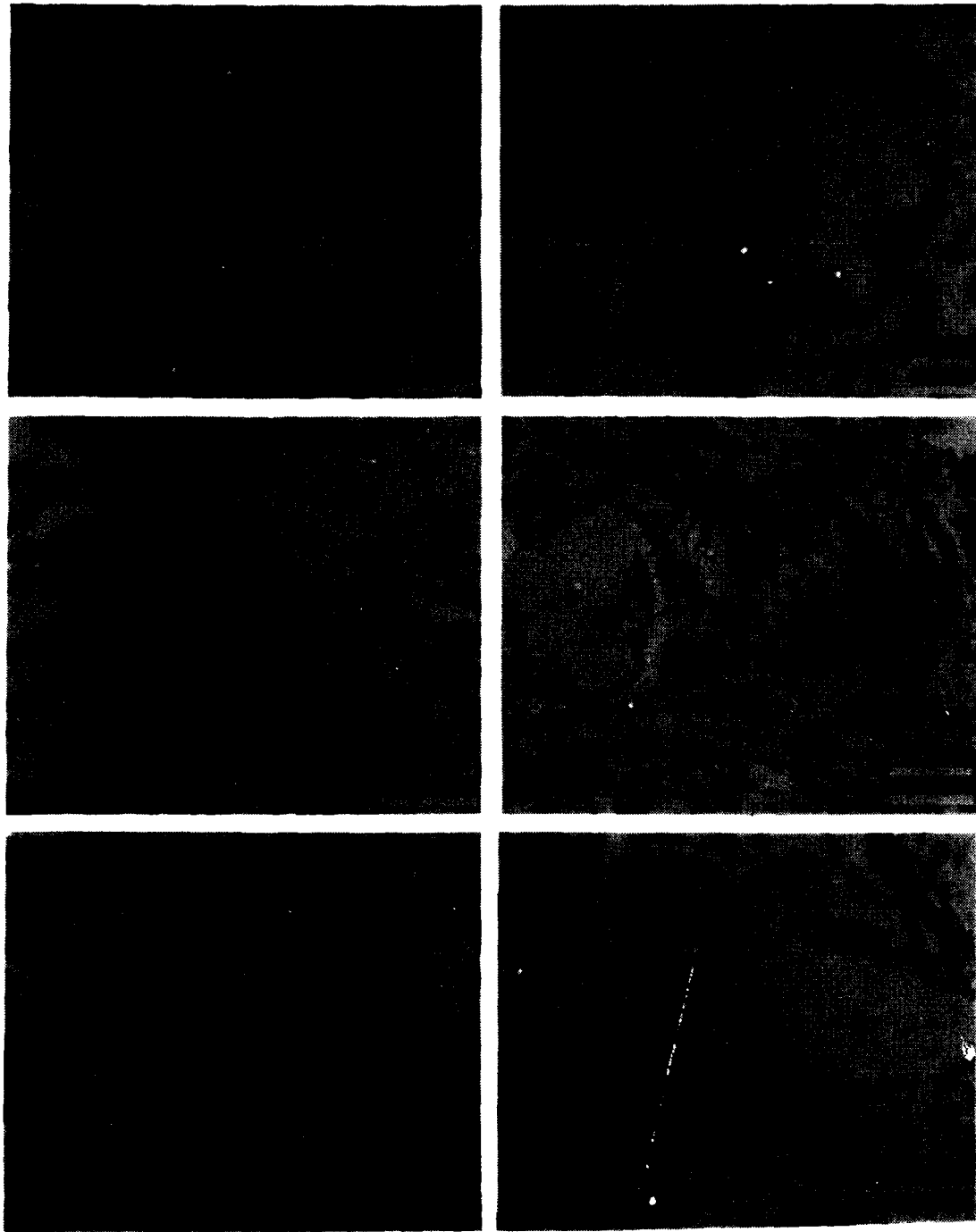


Figure 22. Cross-Sections of Quasi-Expansion Features in Near-Field Samples B-7, B-8, and B-10, Which Have Voids Acting as Conduits for Pore Fluids. These voids (V) are lined with EF and EE particles, and small domains. Micrographs B, C, D, and E show larger particulates which occurred during transport processes within the voids. Tiny black dots in view B are contaminants, possibly hematite, dispersed throughout the resin.

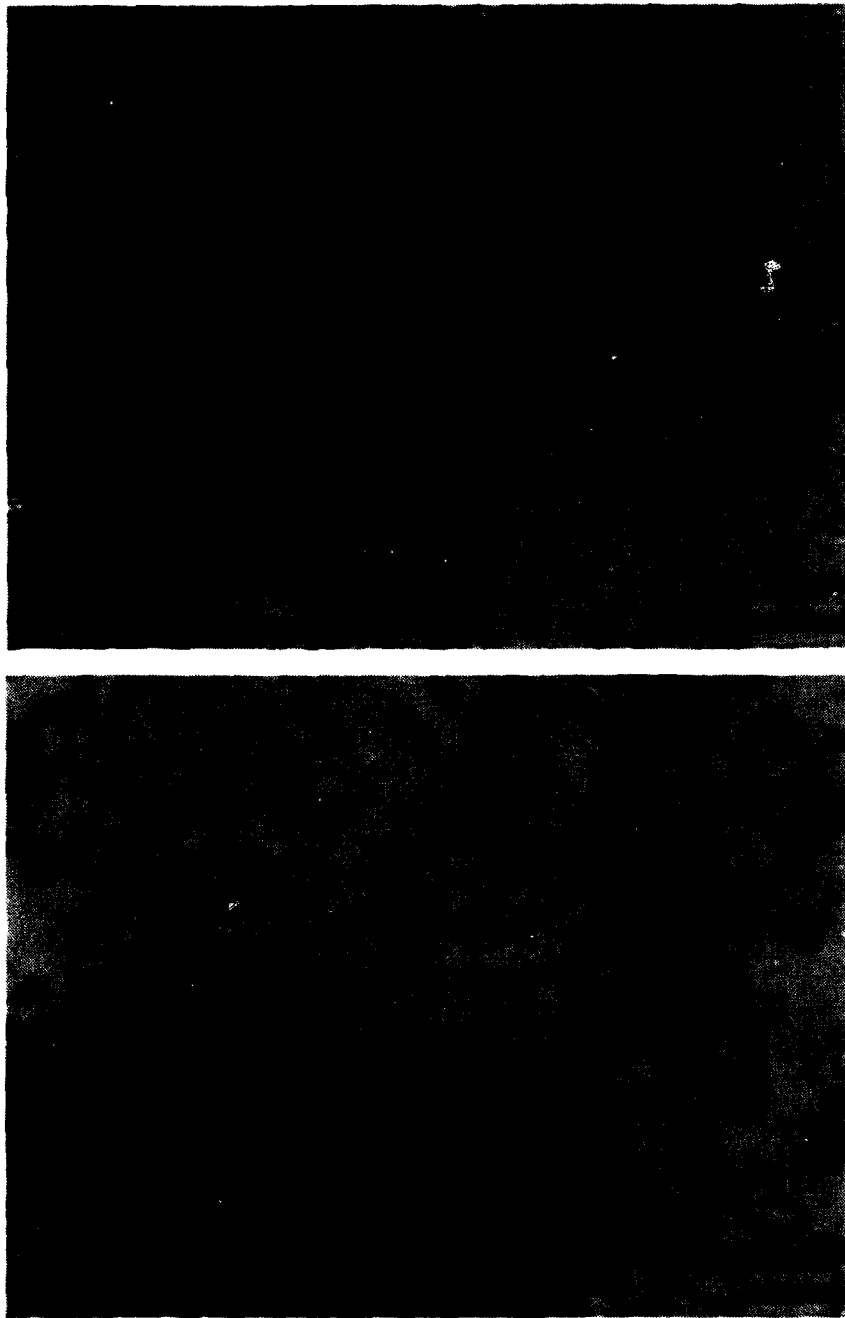


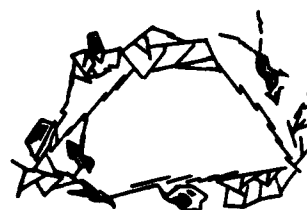
Figure 23. A) Low-Density Smectite Aggregate (S) of Sample B-1 Demonstrating the Onion Skin Layering of Particles Typical of Heated Fabric Samples. The tiny dark dots are innocuous contaminants within the embedding resin. In the upper left portion, the micrograph shows a hole in the resin as a result of a fractured argillite falling out during ultrathin sectioning. This frequent event does not affect the structural integrity of the fabric. B) Two Aggregate Types of Contrasting Densities (A-High Density, S-Low Density) Show the Affinity of Small Domains (Arrows) for the High-Void Smectitic Aggregate (S).



Figure 24. A) Sample B-3 Shows a Low-Density Aggregate, Probably Smectite (S), Surrounded by Onion Skin Layering of EE and EF Particles (Arrows), Beyond Which Are Channels (Dotted Line) for Pore Fluid Transport; B) Small Particles and Domains Line the Low-Density Aggregate (S). Other aggregate types (A) have relatively few particles adhering to their surfaces.

of a mineral's negative charge being balanced by exchangeable cations. Smectite has a high CEC, demonstrated by the onion-skin layering. Beyond the thin layer of particles lining the smectites are micro-channels (Figures 23[a-b] and 24[a]) for the transport of pore fluids and small particles. In Figures 23(b) and 24(b), notice different types of aggregates having the onion-skin around them. These predominately illitic aggregates have a lower CEC, and therefore do not have the tendency to attract small particles of opposite charge. The aligned smectites exist in the RAMA samples as well, but not to as great an extent (see Figure 10).

Another important aspect of this study was to determine by characterization of the fabric if this remolded, reconstituted, illitic-rich red clay sediment is a representative material for laboratory study and testing of geotechnical properties. It has yet to be determined whether this sediment adequately simulates the in situ properties and behavior of the red clay deposits. The RAMA mosaic (Figure 10), composed of twenty micrographs representing an area of  $2,500 \mu\text{m}^2$ , demonstrates the complexity of the clay minerals comprising the fabric. The RAMA mosaic shows the high void ratio fabric typical of Pacific red clays at MPG-1. The prevalent pore spaces are represented by the light background between particles, apparent in all micrographs. Figure 25 (Bennett, 1976) demonstrates models of varying void ratios. RAMA compares to the model with a void ratio of 2.5 (Figure 26); the heated fabric described above looks similar to a medium void ratio of 1.5 to 2.5. From features in the RAMA mosaic and Figure 26, the sediment matrix is dominated by individual particles and small domains behaving as individual particles approximately  $1 \mu\text{m}$  in size. Larger domains ( $2$  to  $5 \mu\text{m}$ ) are fewer in number. This is in contrast to Mississippi-Delta, smectite-rich sediment composed of



Single, Plate-Like Particles and Chains with Very High Void Ratio ( $>3.0$ )



Domain Particles and Chains with High Void Ratio ( $>2.5$ )



Medium to High Void Ratio ( $\approx 1.5-2.5$ )



Low Void Ratio ( $<1.5$ )



Very Low Void Ratio ( $<1.2$ )

Figure 25. Proposed Tentative Clay Fabric Models for Submarine Sediment (Bennett, 1976).

domains as the basic framework of the fabric (Bennett, 1976). In this study the larger domains are, for the most part, illitic argillites fractured during sectioning with a diamond knife. Figure 27(a) is an enlargement of a subrounded "fractillite" (Bryant et al., in progress) typifying an aeolian origin. The fracture patterns are indicative of the direction of knife motion shown by the arrow. Plucking of these grains, leaving holes in the sections because of the brittle

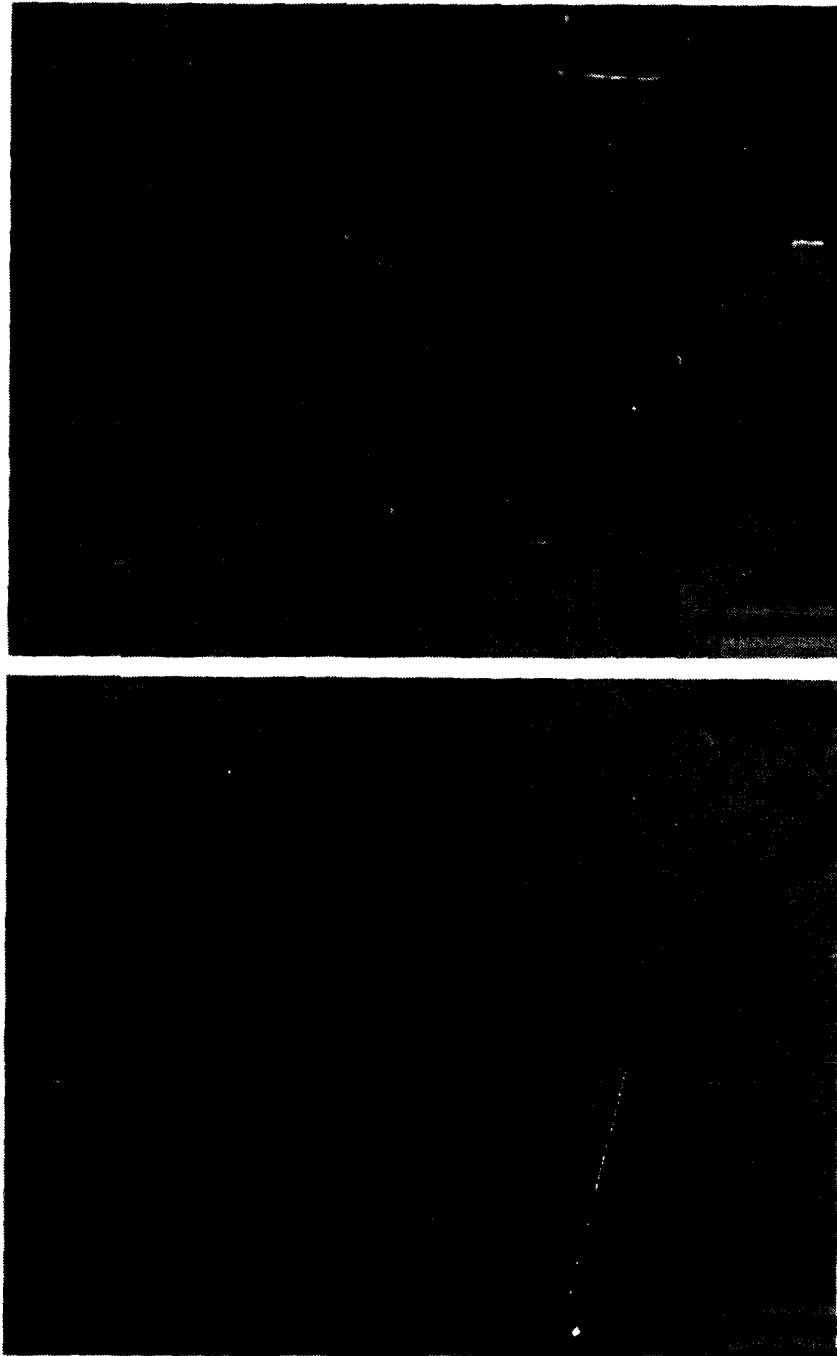


Figure 26. High Void Ratio Nonremolded Fabric of In Situ RAMA Sample Showing Micro-Channels (Dotted Line). The matrix is predominately of particles and small domains (p) arranged stepped FF and EE, and forming short chains (arrows). A) Notice the micro-channels for fluid transport. B) Numerous large argillite domains (L) exist, which fracture during ultrathin sectioning.

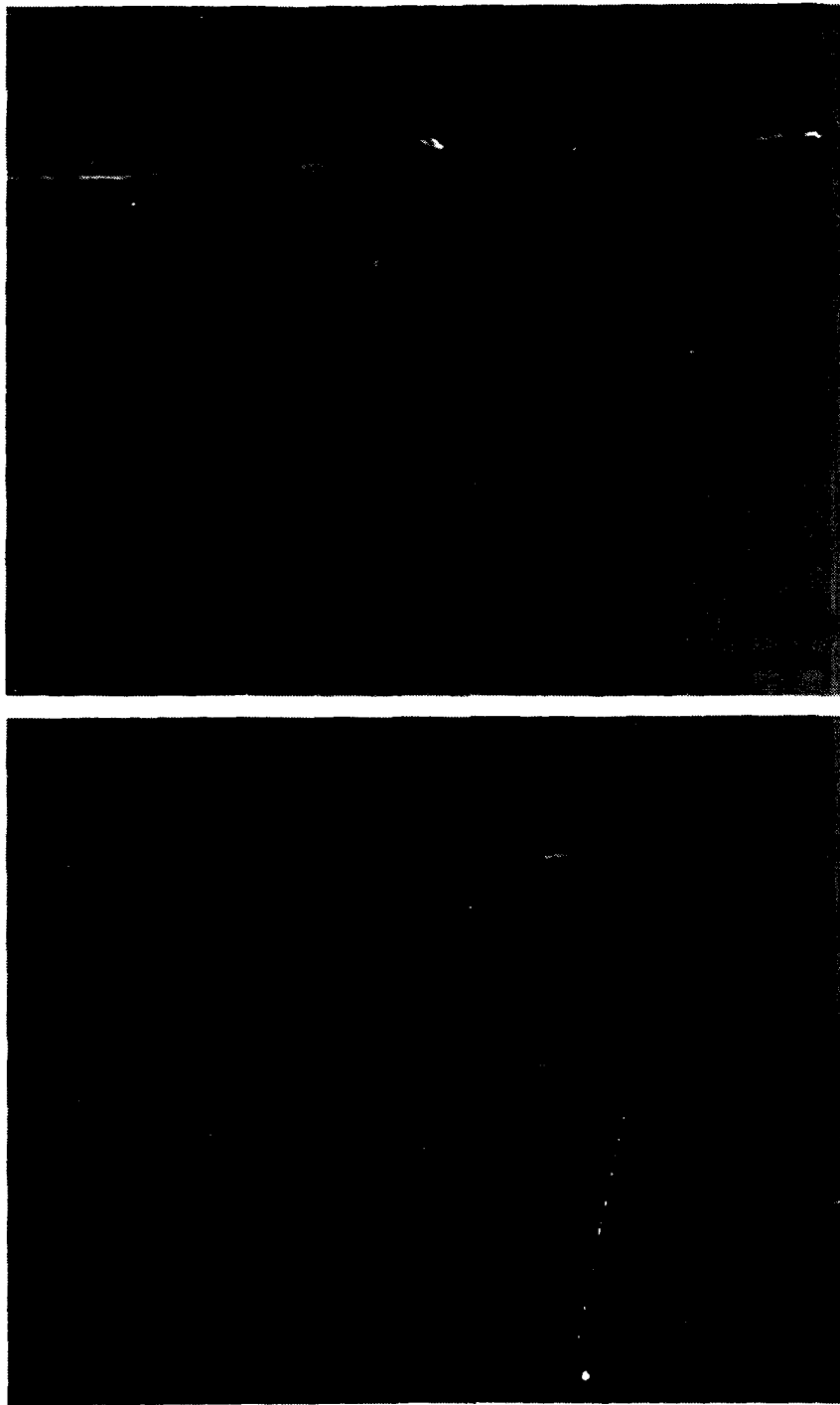


Figure 27. A) A Large Subrounded Argillite (fa) Indicative of Aeolian Origin. The fracture pattern is normal to the direction of sectioning (dark line) with a diamond knife. B) Characteristically fractured large "stringer" argillites (st) are common.

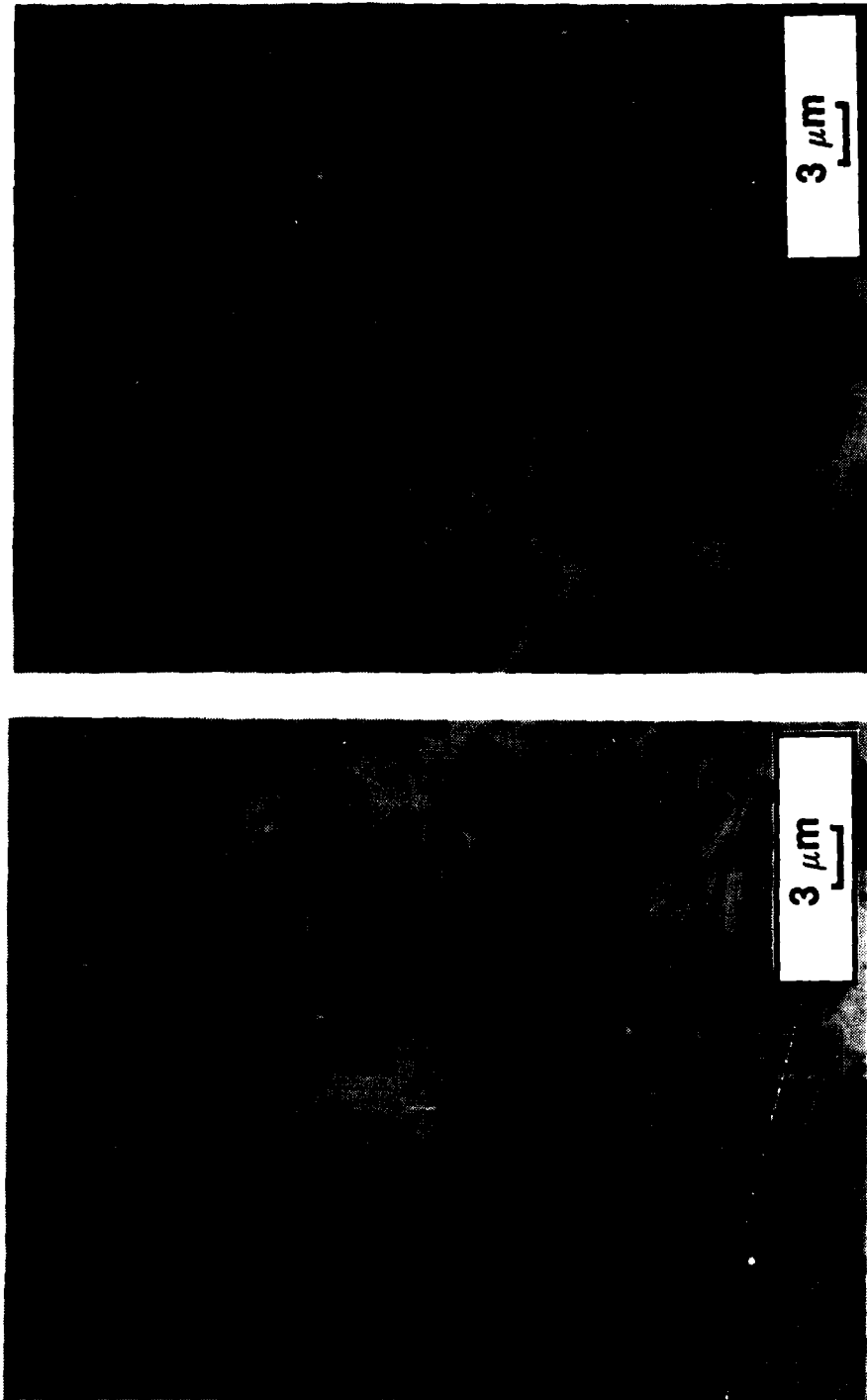


Figure 28. SEM Micrograph of Features Recognizable in Both SEM and TEM. A) Notice the channeling around the large aggregate (A), surrounded by clay platelets probably corresponding to the FF and EE onion-skin particles in Figure 25. B) Particle arrangements creating a high void ration (high-porosity) sediment typical of Pacific red clays, showing EF arrangement and a probable argillite aggregate (A).

nature of the mineral, is common during ultra-thin sectioning, but does not affect the integrity of the fabric (Figures 19[a], 20[b], 23[a], and 24[b]). Elongated or "stringer" fractured illite domains are also common, as seen in remolded sample B4 in Figure 27(b) and in the undisturbed RAMA sample. Also characteristic of this fabric type are naturally occurring channels providing pathways for pore fluid flow evident in the RAMA mosaic. These channels are larger than the micro-channels induced from heating, as seen in the voids in Figure 22. Small channels free of small particles surrounding large domains are pathways for the transport of fluids.

An array of particle configurations typifies the red clays. Common arrangements include edge-to-edge and edge-to-face particle contacts clearly visible in the RAMA mosaic (Figure 10). Many short chains, predominantly stepped face-to-face and edge-to-edge, are prevalent throughout the fabric, with a lesser amount of longer chains and edge-to-face particle arrangements. Several aggregate types are also common. Sample B4 (Figure 23[b]) shows a large, subrounded, oriented, low intra-void aggregate. Adjacent to it is a high void, random aggregate of a different mineralogy. This low-density mineral aggregate, probably smectite, has a characteristic small particle ( $\leq 0.1 \mu\text{m}$ ) size. Flocculated smectite is recognized by its nonaggregate, "fluffy" appearance (Figure 20[b]), and is probably authigenic. In aggregate form, the smectite's structural integrity is demonstrated by the lack of tearing or damage common in the fragile ultra-thin section. This is due to the high adhesiveness of smectite and the numerous particle contacts. All the mineral aggregates are high strength because of the numerous particle contacts and attractive forces at these contacts. Tearing or breakage of the fabric tends to occur between aggregate types, not through them. Chains are also susceptible to breakage, as is evident

in the remolded samples. Pusch (1970) observed aggregates moving as units when subjected to unconfined compression tests and deformation occurring in the connecting links or chains.

Several microfabric features were recognized in both TEM and SEM micrographs. Gross features such as large aggregates (Figure 28) and channeling surrounding the large aggregates could be correlated. The aggregate appears to be "wrapped" in clay platelets comparable to the onion-skin lining of particles and small domains seen in Figures 23 and 24. Also evident were edge-to-face arrangements of particles and some chains of smaller domains having edge-to-edge particle contacts. Argillitic fractured particles were not successfully compared by TEM and SEM. In TEM micrographs these particles have a characteristic fracture pattern from sectioning, which lacks an equivalent in SEM specimens.

#### CONCLUSIONS

Clay fabric was the primary property for assessing the effects of thermal exposure and mechanical disturbances of this illitic sediment to probe insertion, remolding, and varying temperature fields induced during the ISIMU. In response to heating, several characteristics of the reconstituted, laboratory-remolded sediment varied (e.g., shear strength increased and water content decreased). A localized transformation of the clay mineralogy from illite to smectite in the "baked zone" exposed to high temperatures appears to correspond to an increase in the pore fluid potassium levels.

Fabric analysis did show some sediment response from primary remolding during reconstitution of the sediment before the ISIMU. This was evinced by the swirling, twisting, and breakage of longer chains of domains.

Secondary remolding and traction stress caused by mechanical disturbance induced by probe insertion resulted in localized compression features in the near-field fabric samples, demonstrated by an increase in fabric density and alignment of broad bands of particles. The RAMA sample, the control not subjected to remolding or laboratory reconstituting effects, displayed longer, straighter chains of particles forming a less dense fabric.

Thermal forces resulted in quasi-expansion features, small particle-lined voids caused by heated pore fluid flowing through the sediment, pushing small particles aside and forming channel walls. The movement of fluids also brought small particles into contact with the smectitic-type aggregate bearing a large CEC. This resulted in increased layers of stepped, face-to-face particles adhering to the probable smectite aggregates in the near-field, remolded samples. The smectitic aggregates in the RAMA samples had decreased amounts of onion-skin lining of particles.

The complexity of this Pacific red clay fabric type is striking, as seen by the many types of particles, such as large (2- to 5- $\mu\text{m}$ ) argillite domains, aggregates of varying densities, and the larger than 2- $\mu\text{m}$  channels for fluid movement (Figure 10, showing the RAMA mosaic). Various arrangements of particle contacts are observed, including edge-to-edge, stepped face-to-face, and lesser amounts of edge-to-face arrangements. The dominant particle comprising the matrix is small domains  $\sim 1 \mu\text{m}$  in length. The in situ orientation of particles comprising the fabric is random and forms a high void ratio sediment. It is a resilient and durable material whose fabric is remarkably similar to the same sediment-type subjected to the stress of mechanical disturbance and heating. The grain size of the far-field samples varies little from the nonremolded control. Pacific illitic-rich red clay appears to be an excellent material for laboratory use and comparative geotechnical studies of in situ properties of sediment responses.

#### REFERENCES

- APL-UW Engineering Report, ISHTE Simulation, 1982. Applied Physics Laboratory, University of Washington, Seattle, Washington. 60 pp.
- Aylmore, L. A. G., and J. P. Quirk, 1960. Domain or turbostratic structures of clay, Nature, Vol. 187, 1046-1048.
- Baligh, M.M., 1985. Strain path method, Journal of Geotechnical Engineering Vol. 111, no. 9, 1108-1136.
- Bates, R. L., and J. A. Jackson, editors, 1980. Glossary of Geology. American Geological Institute. Falls Church, Virginia, pp. 108 & 481.
- Bennett, R. H., 1976. Clay Fabric and Geotechnical Properties in Selected Submarine Sediment Cores from the Mississippi Delta. Ph.D. dissertation, Texas A&M University, 269 pp.
- Bennett, R. H., W. R. Bryant, and G. H. Keller, 1977. Clay fabric and geotechnical properties of selected submarine sediment cores from the Mississippi Delta. NOAA Professional Paper no. 9, 86 pp.
- Bennett, R. H., W. R. Bryant, and G. H. Keller, 1981. Clay fabric of selected submarine sediments: fundamental properties and models, Jour. of Sed. Petrology, Vol. 51, no. 1, 217-232.
- Bennett, R. H., J. T. Burns, F. L. Nastav, J. Lipkin, and C. M. Percival, 1985. Deep-ocean piezometer probe technology for geotechnical investigations, Journal of Oceanic Engineering, Vol. OE-10, no. 1, 17-22.
- Bennett, R. H., M. H. Hulbert, 1986. Clay Microstructure. International Human Resources Development Corporation (IHRDC). Boston, Massachusetts, 161 pp.
- Bohlke, B. M., and R. H. Bennett, 1980. Mississippi prodelta crusts: a clay fabric and geotechnical analysis, Marine Geotechnology, Vol. 4, pp. 5-82.
- Brewer, R., 1964. Fabric and Mineral Analysis of Soils. John Wiley and Sons, New York, 470 pp.
- Briggs, K., and M. Richardson, 1984. Physical and acoustical properties of surface sediments from venezuela basin: a data report, NORDA Technical Note 238, pp. 15-16.
- Bryant, W. R. (in progress). The physical and mineralogical nature of the red clays of the North Pacific Basin.
- Folk, R. L., and W. C. Ward, 1957. Brazos River Bar: A study in the significance of grain size parameters, Jour. of Sed. Petrology, Vol 27, pp. 3-27.
- Jackson, M. L., 1969. Soil Chemical Analysis-Advanced Course, 2nd edition. Dept. of Soil Science, University of Wisconsin, Madison, Wisconsin.
- Jordan, S. A., 1982. Status report, study of zone of influence effects around the heater. Memorandum to A. J. Silva and ISHTE group. University of Rhode Island, Narragansett, Rhode Island, 8 pp.

- Hollister, C. D., D. R. Anderson, and G. R. Heath, 1981. Subseabed disposal of nuclear waste, Science, Vol. 213, 1321-1326.
- Krumbein, W. C., 1934. Size frequency distributions of sediments, Jour. of Sed. Petrology, Vol. 4, 65-77.
- Lambe, T. W., and R. V. Whitman, 1969. Soil Mechanics. John Wiley and Sons, New York. 502 pp.
- McTigue, D. F., J. Lipkin, and R. H. Bennett, 1986. Consolidation under an isotropic total stress increase: part I, analysis for compressible constituents, Geotechnique 36, No. 1., 1-9.
- Miller, J. B., V. W. Miller, and L. O. Olson, 1982. ISHTe Simulation APL-UW Engineering Report. University of Washington, Seattle, Washington.
- Moon, C. F., 1972. The microstructure of clay sediments, Earth-Science Review, Vol. 8, 303-321.
- O'Brien, N. R., 1971. Fabric of kaolinite and illite floccules, Clays and Clay Minerals, Vol. 19, 353-359.
- Olson, L. O., and J. G. Harrison, 1979. Sea floor system for an in situ heat-transfer experiment, Proceedings Oceans '79. IEEE Pub. 78, CH 14-78-7 OEC, 421-423.
- Percival, C. M., 1982. Laboratory Simulation of a Deep-Ocean In Situ Heat Transfer Experiment, Oceans '82. MTS/IEEE Conference Record, Sept. 20-22, Washington, DC.
- Percival, C. M., 1983. The Subseabed Disposal Program-In Situ Heat Transfer Experiment (ISHTe). SAND80-0202 Sandia National Laboratories, Albuquerque, New Mexico, 47 pp.
- Percival, C. M., D. F. McVey, L. O. Olson, A. J. Silva, 1980. In situ heat transfer experiment (ISHTe), Oceans '80 NTS/IEEE Conference Record, Sept. 20-22, Washington, DC, 567-573.
- Pusch, R., 1970. Microstructural changes in soft quick clay at failure, Canadian Geotech. Jour., Vol. 7, 1-7.
- Randolph, M. S., J. T. Carter, and C. P. Wroth, 1978. Driven Piles in Clay (I): Installation. Modelled as the Expansion of a Cylindrical Cavity. University of Cambridge, Cambridge England, 44 p.
- Silva, A. J., S. J. Criscenzo, S. A. Jordan, and J. A. Babb, 1983. ISHTe Annual Report No. 2. URI Geotechnical Program of the In Situ Heat Transfer Experiment. University of Rhode Island, Narragansett, Rhode Island, 79 pp.
- Sloane, R. L., and J. R. Kell, 1966. The fabric of mechanically compacted kaolinite, Clays and Clay Minerals, Vol. 14, 289-296.
- Smalley, I. J., and J. G. Cabrera, 1969. Particle association in compacted kaolin, Nature, Vol. 22, 80-81.
- Thornton, E. C., 1983. Experimental and Theoretical Modeling of Sediment-Seawater Hydrothermal Interactions at Constant Temperature and in a Thermal Gradient: Implication for the Diagenesis and Metamorphism of Marine Clay and the Subseabed Disposal of Nuclear Waste. Ph.D dissertation, University of Minnesota, 193 pp.
- Van Olphen, H., 1963. An Introduction to Clay Colloidal Chemistry. John Wiley and Sons, New York, 301 pp.

**DISTRIBUTION**

Naval Ocean Research and Development  
Activity (30)  
Seafloor Geosciences Division  
Code 360  
NSTL Station, MS 39529  
Attn: R. H. Bennett (10)  
P. J. Burkett (20)

Texas A&M University  
Department of Oceanography  
College Station, TX 77843  
Attn: W. R. Bryant (20)

Northwestern University (10)  
Material Science and Engineering Dept.  
2145 Sheridan Road  
Evanston, IL 60201  
Attn: W. A. Chiou

University of Rhode Island  
Department of Ocean Engineering  
South Ferry Road  
Narragansett, RI 02882  
Attn: A. J. Silva

Argonne National Laboratories  
9700 South Cass Avenue  
Argonne, IL 60439  
Attn: F. Schreiner

University of Rhode Island  
Graduate School of Oceanography  
South Ferry Road  
Narragansett, RI 02882  
Attn: K. R. Hinga  
M. Leinen

University of Washington (3)  
Ocean Physics Group  
Applied Physics Lab  
1013 Northeast 40th Street  
Seattle, WA 98195  
Attn: L. O. Olson

Woods Hole Oceanographic Institute  
Woods Hole, MA 02543  
Attn: F. Y. Sayles

University of Minnesota  
Department of Geology and Geophysics  
Minneapolis, MN 55455  
Attn: W. Seyfried

US Department of Energy  
Albuquerque Operations Office  
P.O. Box 5400  
Albuquerque, NM 87115  
Attn: W. Forester

3141 S. A. Landenberger (5)  
3151 W. L. Garner (3)  
3134-1 C. H. Dalin (28)  
DOE/OSTI  
6313 L. E. Shephard (10)  
6334 D. R. Anderson  
6334 L. H. Brush  
6334 L. S. Gomez  
9115 C. M. Percival (10)